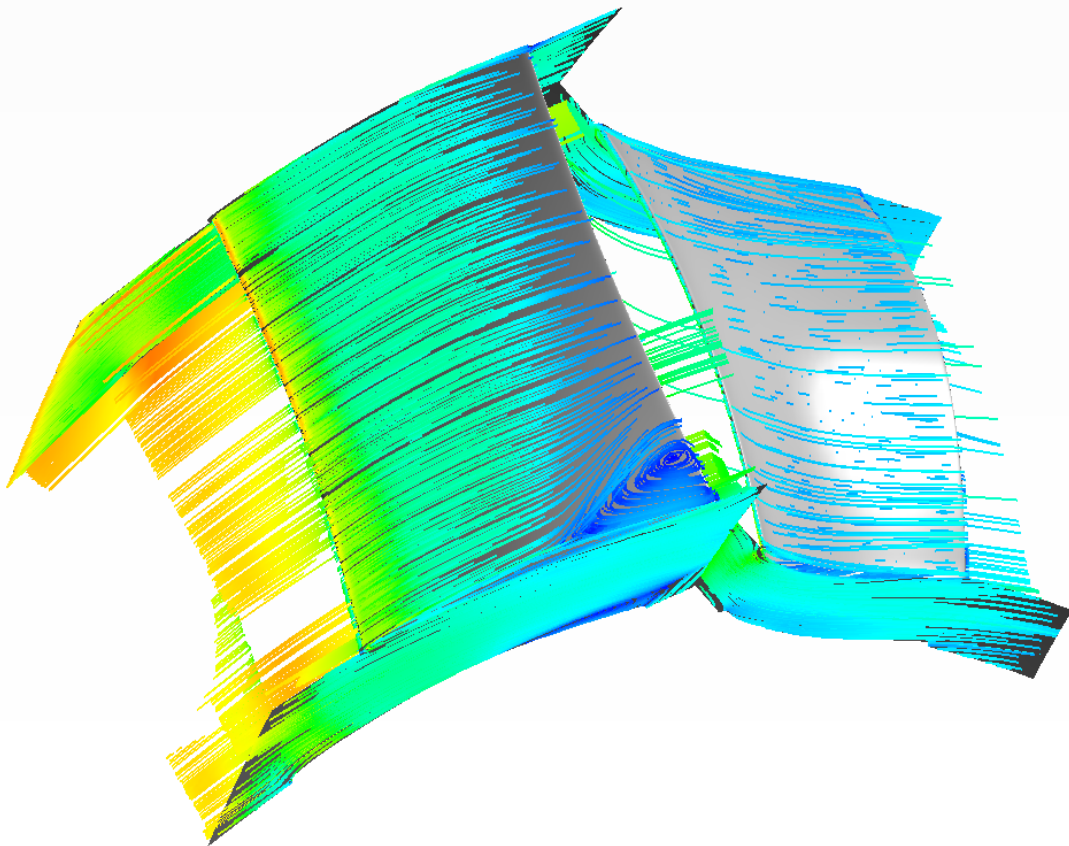




CHALMERS



The Impact of Surface Roughness on Transonic Compressor Performance

Master's thesis in Applied Mechanics

SATHYAVANAN CHINNASWAMY

MASTER'S THESIS IN APPLIED MECHANICS

The Impact of Surface Roughness on Transonic Compressor Performance

SATHYAVANAN CHINNASWAMY

Department of Applied Mechanics
Division of Fluid Dynamics
CHALMERS UNIVERSITY OF TECHNOLOGY
Göteborg, Sweden 2015

The Impact of Surface Roughness on Transonic Compressor Performance
SATHYAVANAN CHINNASWAMY

© SATHYAVANAN CHINNASWAMY, 2015

Master's thesis 2015:40
ISSN 1652-8557
Department of Applied Mechanics
Division of Fluid Dynamics
Chalmers University of Technology
SE-412 96 Göteborg
Sweden
Telephone: +46 (0)31-772 1000

Cover:
Velocity streamline plot with roughness on rotor and stator blades showing separations in near hub region

Chalmers Reproservice
Göteborg, Sweden 2015

The Impact of Surface Roughness on Transonic Compressor Performance
Master's thesis in Applied Mechanics
SATHYAVANAN CHINNASWAMY
Department of Applied Mechanics
Division of Fluid Dynamics
Chalmers University of Technology

ABSTRACT

The increasing necessity for highly efficient engines and low emission standards has steered the need for research into more efficient design and optimization of gas turbines. Surface roughness in the blades of compressors and turbines is one of the factors causing performance deterioration in gas turbines. This study involves the investigation of surface roughness effects on the performance of a research compressor stage through numerical simulations in a commercial CFD code, ANSYS CFX. An initial numerical study on a NACA airfoil was conducted with roughness and validated with the experimental data. It is followed by the implementation of uniform sand grain roughness over the rotor and stator blades of the compressor stage using the surface roughness model available in ANSYS CFX. Two different cases, one with roughness on the rotor and one with roughness on the stator and rotor combination were done. The results from the study shows the reduction in the main performance parameters such as pressure ratio, efficiency and mass flow in the compressor stage. The flow calculations shows an increase in blockage of the flow in the stage with an increase in surface roughness on the blades. Surface streamlines shows the influence of surface roughness on the separation over the suction side of the stator and the regions near the hub in the rotor.

Keywords: Computational Fluid Dynamics, Turbomachinery, Wall roughness, Turbulence, Axial compressor, Technical roughness, Sand grain roughness, Boundary layer effects, Transition, Blockage, Wall functions.

ACKNOWLEDGEMENTS

This Master Thesis has been carried out in cooperation with Division of Fluid Dynamics at Chalmers University of Technology and GKN Aerospace Sweden, Trollhättan. I would like to show my gratitude:

- Niklas Andersson, Examiner at Chalmers University of Technology for the opportunity and valuable support for executing this project.
- Marcus Lejon, PhD Student and Supervisor at Chalmers University of Technology for his valuable guidance and technical feedback throughout the project.
- Lars Ellbrant, Supervisor at GKN Aerospace Sweden for his technical guidance and support.
- Division of Fluid Dynamics for the administrative support and workplace with computational resource to carry out this project at Chalmers University of Technology.
- Chalmers Centre for Computational Science and Engineering, Göteborg for providing the computational resources.

I also thank my family and friends specially Ragnar Hellsvik for their motivation and support during the project.

Sathyavanan Chinnaswamy, Göteborg , Jun 2015

NOMENCLATURE

Roman

p	pressure
A_{eff}	effective throttle area
R_a	measured roughness parameter
k_s	equivalent sand grain roughness
T	temperature
k	turbulent kinetic energy
N	shaft speed
M	Mach number
Re	Reynolds number
y^+	dimensionless wall distance
u^+	dimensionless velocity
k_s^+	non-dimensional roughness height

Greek Symbols

ε	turbulent dissipation rate
μ	dynamic viscosity
μ_t	turbulent eddy viscosity
ρ	density
γ	specific heat ratio
η	polytropic efficiency

Subscripts

0	total condition
nh	near hub
nt	near tip
ms	mid span
RMS	root mean square
zd	peak to valley
CLA	center-line average
a	arithmetic average

Miscellaneous symbols

–	ensemble average
---	------------------

Abbreviation

CFD	Computational Fluid Dynamics
RANS	Reynolds Averaged Navier-Stokes
LES	Large Eddy Simulations
FOD	Foreign Object Damage

Contents

Abstract	i
Acknowledgements	ii
Nomenclature	iii
1 Introduction	1
1.1 Background	1
1.2 Objective	3
1.3 Scope	3
1.4 Thesis Outline	3
2 Theory	4
2.1 Compressor performance parameters	4
2.1.1 Efficiency	4
2.1.2 Total Pressure Ratio	4
2.1.3 Mass flow	4
2.2 Compressor Map	5
2.3 Surface roughness	6
2.3.1 Losses due to roughness	6
2.4 Boundary Layer effects	7
2.5 Aerodynamic coefficients for airfoil	8
2.6 Numerical Modelling	9
2.6.1 Control volume discretisation	9
2.6.2 Turbulence modelling	9
2.6.3 k- ϵ model	10
2.6.4 Scalable wall functions	10
2.7 Wall Roughness Modeling	10
2.7.1 Roughness modeling in CFX	11
2.7.2 Roughness modeling in Fluent	11
2.8 Limitations in CFD involving turbomachinery	12
3 Numerical study of an airfoil	13
3.1 Numerical 2D Simulations	13
3.1.1 Geometry and mesh generation	13
3.1.2 Boundary conditions	14
3.1.3 Simulations	15
3.2 Results and Validation	15
3.3 Transition simulations	18
4 Numerical study of a compressor stage	20
4.1 3D Stage Simulations	20
4.1.1 Geometry and grid generation	20
4.1.2 Boundary Conditions	20
4.1.3 Simulations	21
4.1.4 Mesh Independency study	23
4.2 Stage simulation results	24
4.3 Roughness over hub and shroud region	30
4.4 Transition influence on the Stage performance	32

5 Conclusion	34
5.1 Summary and Conclusion	34
5.2 Future work	34

References

Chapter 1

Introduction

The application of gas turbines in industries has increased rapidly since its development and mainly used in the aviation and power generation sectors. Aircraft engines are, unlike industrial gas turbines, exposed to very different environments which makes them more likely to be affected by performance degradation due to external factors. Thus, there is an increasing need for highly efficient aircraft engines with less performance deterioration in operation and lower emissions. From the financial aspects, gas turbines with less performance deterioration have a competitive advantage for gas turbine manufacturers. This paves the urge for the better design optimization and efficiency in the gas turbines. The types of performance degradation in gas turbines includes recoverable, non-recoverable and permanent deterioration which encompasses erosion, fouling, increase in vane, blade clearances and manufacturing deviations [25]. The factors that causes the performance degradation due to surface roughness in an aircraft engine comprise of erosion of blades due to runway debris, foreign object damages(FOD), dirt, corrosion and abrasion. This increase in surface roughness decreases the performance in terms of mass flow, pressure ratio, fuel consumption and thrust. For a typical engine, there is a certain limit in the blade surface roughness to have minimum flow losses. The manufacturing of such blades has the downside of increasing cost[15]. The large fuel cost for a commercial airplane and the fact that the performance deterioration from erosion accounts for 45%, blade and vane radial clearance 22%, seal radial clearance 5% and remaining 20% due to miscellaneous causes [25] highlights the importance of engine manufacturer considering surface roughness. So the need for investigating surface roughness is not restricted only in minimizing performance deterioration but also to reduce the manufacturing and maintenance cost for the manufacturers.

1.1 Background

A general overview of the performance deterioration in gas turbines is reported by Meher et al[25]describing the types of degradation and causes of such degradation. Numerous research has been done to study the influence of surface roughness on the performance of turbomachinery. Nikuradse(1933) is the pioneer in the investigation of surface roughness involving pipe flows for different sand grain sizes. A research conducted by Suder et al [11] investigated the influence of roughness on a high speed axial compressor rotor by rough coating with finish of 2.54-3.18 rms μm which accounted for 9% reduction in pressure ratio across the rotor. A smooth coating was done on the rotor to remove the effect of thickness and surface roughness. Comparing this with the rough coating resulted in half the performance deterioration. He also investigated numerical predictions of the performance deterioration using a quasi-three-dimensional Navier-Stokes flow solver with a roughness model which indicated the thickening of boundary layers due to added roughness.

Bammert & Woelk [6] performed quantitative measurements on a three stage model axial compressor to evaluate the effect of blading surface roughness on the aerodynamic behavior and its operating characteristics. The blading comprises of inlet guide blades and three stages with the arrangement of rotor guide blades. The measurements were carried out for smooth and uniform rough blading with sand grain roughness range of $60\mu\text{m}$, $100\mu\text{m}$ and $180\mu\text{m}$ which were implemented by corresponding emery grains which corresponds to sand grains. Their work concluded the roughness size of $180\mu\text{m}$ on the blading showed decrease in efficiency of 13% and reduction of 30% in achievable static pressure ratio as compared to the smooth blading. It was found that there is a risk of crossing the surge line during operation due to the narrowing of the characteristic field between the surge line and the throttling line for the roughened blading. Bammert & Sandstede [15] carried out measurements on a 4 stage air turbine to study the aerodynamical and thermodynamical behaviour of the turbine under the influence manufacturing tolerances and surface roughness of the turbine blades. For partly rough blade surfaces, they found that losses were more influenced by the rear part of the suction side than the front. They observed a reduction of 17.3 % in the power output of the turbine due to roughness in the blade surfaces with relative roughness of $k/l=10.6\text{e-}03$ which was the highest roughness size considered. Im et al [21]reported the influence of leading edge roughness and Reynolds number on profile loss using compressor

cascade experiments. They recorded reduction in profile loss at $Re=210,000$ and the loss increased drastically for $Re=640,000$.

Moreover Leipold et al [17] conducted experiments using a highly loaded compressor cascade to study the influence of technical roughness due to the manufacturing processes on the losses in the compressor cascade. They studied the effect of varying Reynolds number on the isentropic Mach number distribution and local total pressure loss for smooth and rough blade cascade. The actual technical roughness was engraved on the surface of a copper sheet with a factor of ten enlarged copy of actual roughness since the compressor blades are enlarged to increase the spatial resolution of the flow phenomena. They also studied the boundary layer development due to roughness using laser-two-focus anemometry and one-dimensional hot wire anemometry. The effect of roughness was less on the isentropic Mach number distribution for all Reynolds number variation. In contrast, the total pressure loss increased for higher Reynolds number due to high losses because of roughness impact on the turbulent separation on the suction side. Millsaps et al [10] investigated the performance degradation due to the effects of surface roughness for different Reynolds number and Location through experiments in a low-speed linear compressor cascade. The tests were conducted for different roughness magnitudes R_a of 0.38, 1.70, 2.03, 2.89 μm which were centreline averaged roughness values. The test results showed increase in loss and blade loading became sensitive to roughness at Reynolds number greater than 550,000. Based on location, it was concluded that the suction side of the cascade was more sensitive to roughness than the pressure side and also it increases with Reynolds number.

Back et al [9] presented results from the experiments conducted in a compressor cascade to investigate the influence of roughness on the aerodynamic performance parameters such as axial velocity, deviation and total pressure loss. For the minimum sand grain roughness value tested of $850\mu m$, they found a reduction of 5.4% in axial velocity ratio and 217% increase in total pressure loss. They found that the losses were the most sensitive to roughness than the other parameters considered. Elrod et al [13] studied the collective effect of surface roughness, freestream turbulence and incidence angle on the performance of compressor cascade tests. The conclusion from the tests was that increase in roughness caused rise in total pressure loss coefficient and it reduced for larger free stream turbulence. Schäffler [20] investigated the influence of Reynolds number and blade surface roughness in multi-stage axial compressors both analytically and experimentally. The study showed that the technical blade roughness formed by different manufacturing methods have influence on the critical roughness Reynolds number. Discussions were made on the boundary layer flow development within different Reynolds number regime.

Experiments and Numerical calculations by Gbadebo et al investigated the effect of roughness on 3D separation in a compressor stator and followed by stage performance. The tests showed that a hub corner separation caused by roughness in the stator lead to high loss, increased blockage and a significant total pressure loss in the stage. The numerical predictions for the boundary layer development and performance losses were under-predicted when compared with experimental data. A typical study was done by Syverud et al [18] to investigate the impact of roughness on axial compressor performance by comparing the test results from a GE J85-13 test program with the analytical predictions involving a equivalent Reynolds correction model and blade profile loss model. The roughness was simulated in tests by saltwater ingestion on the engine compressor. Their study showed a significant reduction in flow coefficient due to the roughness caused by fouling. Kang et al [19] studied the effect of roughness on compressor and turbine stage numerically using a commercial code TascFlow. The study was conducted on the third stage of a low speed research compressor designed by GE. They reported reduction in efficiency due to roughness in both turbomachines. Aerodynamic loss due to roughness with varying Reynolds number on turbine blades was reported by Tao et al [23] through numerical simulations of a turbine cascade. Boundary layer thickening and noticeable increase of 129% in total pressure loss coefficient at $Re=300,000$ was noticed compared to the smooth blade. Moreover Yang et al [26] also did a numerical study on NASA rotor37 in CFX by implementing three different roughness values $R_a=50, 100$ and $150\mu m$. They noticed 5.37% decrease in pressure ratio for the minimum R_a value. Recently Chen et al (2013) [16] did a numerical investigation of roughness effects on the NASA Stage35 rotor blades. They added roughness in different regions of the blade and performance deterioration due to the same. Validation with experimental results were done with a error margin of 3%. Roughness on the suction surface was predicted to have more influence than the pressure side and the roughness near trailing edge was less sensitive than other regions of the blade because of thicker boundary layer.

1.2 Objective

The primary objective of this project is to study the effects of surface roughness on axial compressor performance which results from the manufacturing processes such as milling etc, using existing surface roughness models in commercial CFD solver codes. The effects of surface roughness on performance parameters such as total pressure ratio, polytropic efficiency and mass flow are to be investigated. At first numerical 2D RANS(Reynolds Averaged Navier Stokes) computations will be carried out for different existing models with wall function approach on a NACA airfoil and compared with experimental results. This is to be followed by 3D RANS computations for a research transonic compressor stage geometry in ANSYS CFX using the surface roughness model chosen from the conclusions from the preliminary study on a NACA airfoil.

1.3 Scope

The main focus of the study is to investigate the effect of surface roughness on the performance of an axial compressor stage using existing models. Uniform surface roughness is applied to different blade surfaces to see its effect on the performance. Steady state simulations are done for the performance evaluations. Tip clearances are not included in the simulations.

1.4 Thesis Outline

This section explains the layout of the thesis report. In Chapter 2, the fundamental equations governing the flow, turbulence and wall roughness modeling are described. The basic compressor performance characteristics are also covered. It is followed by Chapter 3 where the approach for a 2D airfoil analysis and a 3D stage analysis including the mesh generation, boundary conditions and solver set-up are explained. In Chapter 4, the results from the airfoil analysis and stage simulations are presented with plots and numerical values. Surface streamline plots showing the separations in the stage rotor and stator blades and supporting reasons are discussed in the same section. Summary and conclusions obtained from the investigations for the axial compressor stage are presented in Chapter 5.

Chapter 2

Theory

This chapter describes the basic aspects of the compressor performance characteristics and the numerical modeling. The basic governing equations of the RANS model and details of the turbulence model is explained briefly. The background of the surface roughness types and the related losses are covered. Discussion on numerical part of the wall roughness modeling in ANSYS CFX and ANSYS Fluent commercial CFD packages has been done and also a general overview of the limitations in performing CFD simulations within turbomachinery is briefed.

2.1 Compressor performance parameters

2.1.1 Efficiency

A typical axial compressor stage consists of rotor row followed by a stator row. When the flow passes through a stage, work is done on the flow by the rotor. The polytropic efficiency is given as

$$\eta_p = \frac{\gamma - 1}{\gamma} \frac{\ln\left(\frac{P_{02}}{P_{01}}\right)}{\ln\left(\frac{T_{02}}{T_{01}}\right)} \quad (2.1)$$

where P_{01} and P_{02} are the total pressure at the inlet and outlet stations respectively, T_{01} and T_{02} are the total temperature at the inlet and outlet respectively, γ is the ratio of specific heats.

2.1.2 Total Pressure Ratio

The total pressure rise across the compressor stage is given as the total to total pressure ratio across the stage which reads as

$$r = \frac{P_{02}}{P_{01}} \quad (2.2)$$

where P_{01} and P_{02} are the total pressure at inlet and outlet stations respectively

2.1.3 Mass flow

In turbomachinery applications, non dimensional mass flow rate which is otherwise called as capacity [29] is used for the performance assessment. The compressible flow relation between stagnation and static pressure is given as

$$\frac{P_0}{P} = \left(\frac{T_0}{T}\right)^{\frac{\gamma}{\gamma-1}} = \left(1 + \frac{\gamma-1}{2} M^2\right)^{\frac{\gamma}{\gamma-1}} \quad (2.3)$$

By using the equation of state $P = \rho RT$, and relation from eq 2.3 we get the non dimensional mass flow as

$$\frac{\dot{m} \sqrt{RT_0}}{A_n P_0} = \sqrt{\gamma} M \left(1 + \frac{\gamma-1}{2} M^2\right)^{\frac{-(\gamma+1)}{2(\gamma-1)}} \quad (2.4)$$

In case of compressor with variable area nozzle exit [8], the equation 2.4 can be expressed in terms of total pressure ratio by multiplying with stagnation reference conditions and using stagnation conditions in eq 2.3 we get

$$\dot{m} = C \frac{A}{\cos \theta} r^{1 - \frac{\gamma-1}{2\gamma}} M_2 \left(1 + \frac{\gamma-1}{2} M^2\right)^{\frac{-(\gamma+1)}{2(\gamma-1)}} \quad (2.5)$$

where

$$C = \sqrt{\frac{\gamma}{RT_{01}}} P_{01} \quad (2.6)$$

r is the total pressure ratio and the corrected mass flow can be calculated as

$$\dot{m}_{corrected} = \dot{m} \sqrt{\frac{T_0}{T_{0ref}} \frac{p_{0ref}}{p_0}} \quad (2.7)$$

2.2 Compressor Map

A compressor map is a chart which gives information about the performance of the compressor at design and off design conditions. This is typically a plot between total-total pressure ratio along y-axis and corrected mass flow along the x-axis for different corrected rotational speeds. The working or throttle line is the locus of operating points of the compressor for a variation of rotational speeds and can be varied using a bleed system or variable inlet guide vanes. The map contains the surge line determining the operating range before surge which is sudden flow reversal occurring in compressors. It can also contain efficiency(η) variation with mass flow shown as contours.

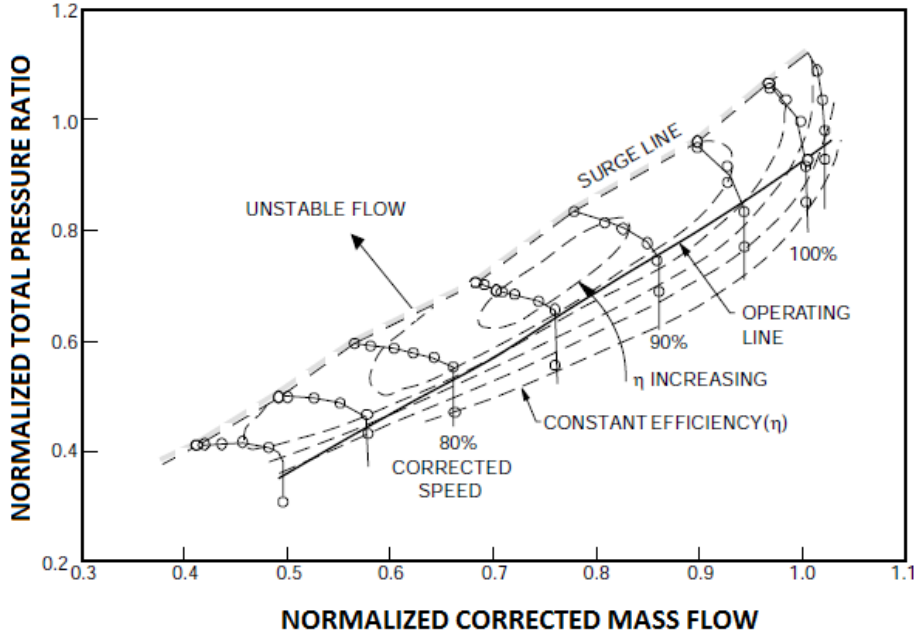


Figure 2.1: *Typical Compressor Map*

The corrected rotational speed is given as,

$$N_{corr} = N \sqrt{\frac{T_{0ref}}{T_0}} \quad (2.8)$$

where N is the rotational speed in rev/min.

The throttle area which is constant along the operating line can be calculated from eq 2.5

$$A_{op} = \frac{\dot{m}}{C r_{op}^{1-\frac{\gamma-1}{2\eta\gamma}} M_{op,2} \left(1 + \frac{\gamma-1}{2} M_{op,2}^2\right)^{\frac{-(\gamma+1)}{2(\gamma-1)}}} \quad (2.9)$$

2.3 Surface roughness

Surface roughness defines the quality of a surface which depends on height of the peaks on the irregular surface, size and distribution on the surface. When the peaks are small below the laminar sub layer then the surface is considered hydraulically smooth otherwise the surface is considered rough. The common types of roughness are corrugated roughness, ribbon-type roughness elements and idealized sand grain roughness. The blade surface roughness in turbomachines uses the equivalent sand grain roughness which was defined in Schlichting [30]. The measured roughness parameters are defined in different forms such as R_a or R_{CLA} , R_{RMS} and R_{zd} [7].

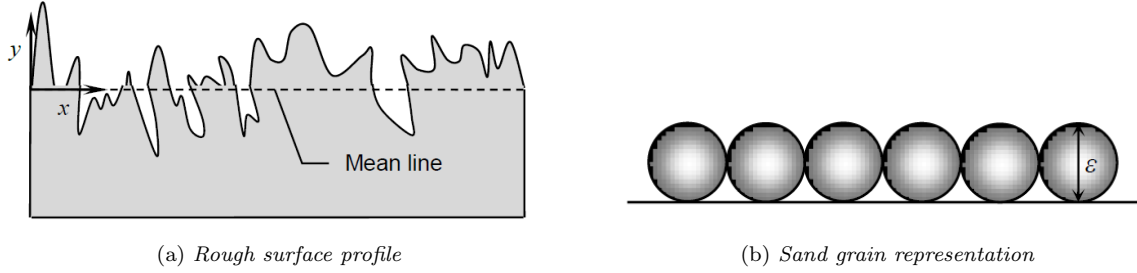


Figure 2.2: Representation of roughness from Thomas et al[7]

R_a , arithmetic average or R_{CLA} , center-line average of the roughness values are given as

$$R_a = \frac{1}{n} \sum_{i=1}^n |y_i| \quad (2.10)$$

where y_i is the distance of the average height of the mean line for measurement i for n number of measurements respectively.

R_{RMS} is the root mean squared values of the roughness calculated as

$$R_{RMS} = \sqrt{\frac{1}{n} \sum_{i=1}^n y_i^2} \quad (2.11)$$

R_{zd} is the peak to valley measurement of the roughness values.

$$R_{zd} = \frac{1}{5} \sum_{i=1}^5 (R_{pi} - R_{vi}) \quad (2.12)$$

where R_{pi} and R_{vi} are maximum distance above and below the mean line for any five measurements.

2.3.1 Losses due to roughness

The general purpose of an axial compressor is to get a rise in stagnation pressure of the flow which is achieved by doing work on the flow by the rotor. Various losses occur during this process of pressure rise in the compressor. The primary sources of the loss are profile losses, losses due to end wall boundary layers and tip clearances and shock losses[32]. The addition of roughness accounts for losses such as increased profile loss due to the thickening of boundary layers, three dimensional separation losses, losses influenced by end wall boundary layers[18]. The surface roughness increases the skin friction and fluctuations in turbulence near wall region which gives rise to rapid development of turbulent boundary layer. The increase in surface roughness also induce earlier transition which along with the thickening of the boundary layers due to roughness are depicted in fig 2.3.

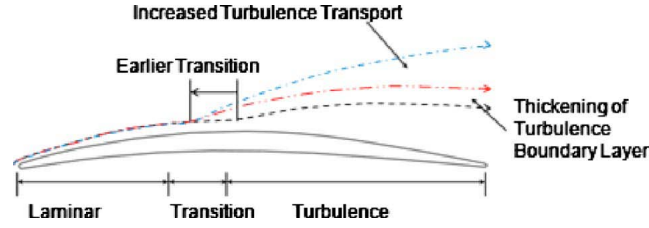


Figure 2.3: *Thickening of boundary layer from Back et al [9]*

2.4 Boundary Layer effects

In general turbulent flows are greatly influenced by the walls as they are the main source for generation of vorticity and turbulence. The flow in the boundary layer has a major effect on the entropy generation in the flow. So wall modelling affects the prediction of the wall-bounded flows. Based on several experiments, near wall region is divided into three layers

- Viscous sublayer
- Buffer layer
- Log law layer

Viscous sublayer is the innermost layer where the domination of viscosity over inertial forces is seen for the momentum. Log layer is the outermost layer or overlap layer where the flow is fully turbulent and is mostly governed by inertial forces. The buffer layer is the blending region with equal importance from viscosity and inertial forces[33]. The subdivisions of the near wall region are depicted in the fig 2.4 below, The general

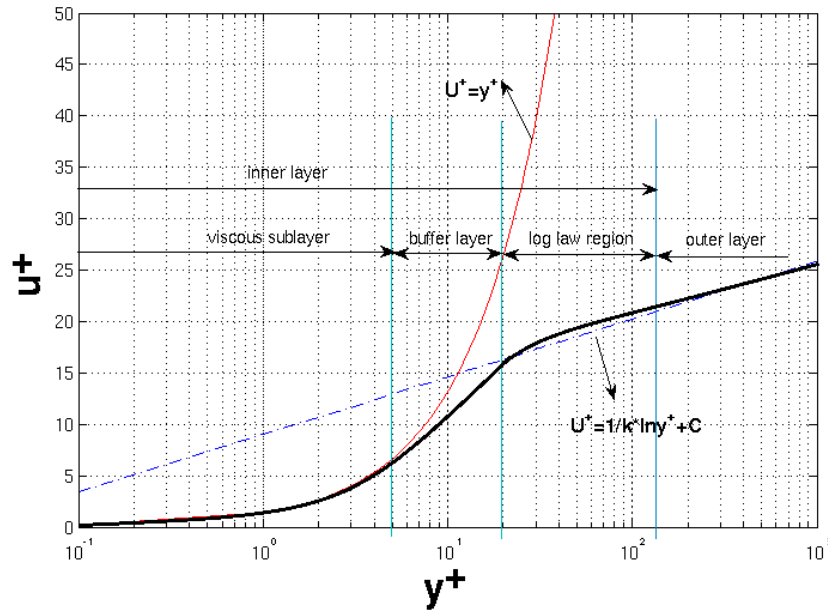


Figure 2.4: *Subdivisions of near wall region*

logarithmic law of the wall reads as

$$\lim_{y^+ \rightarrow \infty} u^+(y^+) = \frac{U_t}{u_\tau} = \frac{1}{\kappa} \ln y^+ + C^+ \quad (2.13)$$

where Von Karman constant, $\kappa=0.41$, $C^+ = 5.0$ for smooth wall, u^+ is the near wall velocity, U_t is the velocity tangent to the wall and y^+ is the non dimensional distance from the wall given as

$$y^+ = \frac{y u_\tau}{\nu} \quad (2.14)$$

where u_τ is the frictional velocity defined in eq 2.15 and ν is the kinematic viscosity

$$u_\tau = \left(\frac{\tau_w}{\rho} \right)^{\frac{1}{2}} \quad (2.15)$$

where τ_w is the wall shear stress and ρ is the density of the fluid. The divisions in the wall layer are tabulated in table 2.1 with the y^+ range.

Table 2.1: Law of the wall

pure viscous sublayer	$0 \leq y^+ < 5$	$u^+ = y^+$
buffer layer	$5 < y^+ < 30$	
log law layer	$30 < y^+$	$u^+ = \frac{1}{\kappa} y^+ + C^+$

Schlichting[30] introduced the term sand grain roughness assuming the wall is layered with a pack of spheres shown in fig 2.2b and the diameter of the spheres, k_s is the equivalent sand roughness height which gives a measure of the surface roughness of the wall. h_s and ε are often used as nomenclature for the sand grain roughness height. To describe the effect of roughness on the law of the wall, a non dimensional roughness height is introduced which is given as

$$k_s^+ = \frac{k_s u_\tau}{\nu} \quad (2.16)$$

In general roughness introduces large perturbations in the laminar flow[30]. For laminar flows roughness favours for laminar-turbulent transition which causes transition to occur at lower Reynolds number than the smooth wall. The roughness is divided into three regimes based on equivalent sand grain roughness as follows

Table 2.2: Roughness regimes

hydraulically smooth	$0 \leq k_s^+ < 5$
transition region	$5 < k_s^+ < 70$
fully rough	$70 \leq k_s^+$

The equivalent sand grain roughness estimated from the measured surface roughness which was discussed in section 2.3 are tabulated in table 2.3

Table 2.3: Equivalent sand grain roughness correlation with measured surface roughness [7]

Measured roughness parameter	Equivalent sand grain roughness, k_s
R_a	$k_s = 5.863 R_a$
R_{RMS}	$k_s = 3.100 R_{RMS}$
R_{zd}	$k_s = 0.978 R_{zd}$

2.5 Aerodynamic coefficients for airfoil

The aerodynamic characteristics of an airfoil is mainly assessed using aerodynamic coefficients. In general, the resultant forces over an airfoil are divided into two components, lift force component acting perpendicular to the flow direction and a drag force component acting parallel to the flow direction. The non-dimensional lift and drag coefficients are calculated by using the lift and drag forces respectively. The equations for lift and drag force calculation and their respective coefficients are listed below.

$$C_l = \frac{l}{\frac{1}{2} \rho V^2 c} \quad (2.17)$$

$$C_d = \frac{d}{\frac{1}{2} \rho V^2 c} \quad (2.18)$$

where the c is the chord length of the airfoil, ρ is the density, V is the velocity of the flow, l is the lift force per unit span and d is the drag force per unit span.

2.6 Numerical Modelling

The CFD code solves Navier-Stokes equations [eq 2.20- eq 2.22] for a defined control volume using a numerical method. The control volume is divided into elements (cells) for which the equations are solved. The result is then analysed using qualitative and quantitative methods. This is a very general explanation of the CFD workflow, the specific method include discretisation of control volume, Reynolds averaging, turbulence modelling, post-processing methods etc.

The equations that describe the transport processes of momentum, heat and mass transfer are the governing equations. The governing equations represents the law of conservation of mass, momentum and energy transfer in a fluid flow. The governing equations are given in conservative form.

The general form of continuity equation is given as

$$\frac{\partial \rho}{\partial t} + \nabla \cdot (\rho \vec{v}) = S_m \quad (2.19)$$

where S_m is the source term[33].

The momentum equation is given as

$$\frac{\partial \rho \vec{v}}{\partial t} + \nabla \cdot (\rho \vec{v} \vec{v}) = -\nabla p + \nabla \cdot (\bar{\tau}) + \rho \vec{g} + \vec{F} \quad (2.20)$$

where p is the static pressure, $\bar{\tau}$ is the stress tensor and $\rho \vec{g}$ and \vec{F} are the gravitational and external body forces[33]. The stress tensor is given by

$$\bar{\tau} = \mu \left[(\nabla \vec{v} + \nabla \vec{v}^T) - \frac{2}{3} \nabla \cdot \vec{v} I \right] \quad (2.21)$$

The energy equation is given as [28]

$$\frac{\partial \left[\rho \left(e + \frac{v^2}{2} \right) \right]}{\partial t} + \nabla \cdot \left[\rho \left(e + \frac{v^2}{2} \right) \vec{v} \right] = \rho \dot{q} + \nabla \cdot (k \nabla T) - \vec{v} \cdot \nabla p + \vec{v} \cdot (\nabla \cdot (\bar{\tau})) + \rho f \cdot \vec{v} \quad (2.22)$$

2.6.1 Control volume discretisation

The control volume has to be discretised before solving the equations for the computational domain. The discretisation or mesh generation in most CFD applications has been done in two ways, structured and unstructured. The unstructured grid is made by placing the grid points in an irregular manner over the flow field. The structured grid is the one with regular arrangement of grid points over the domain. Each one has its advantages and disadvantages which depends on the application. The structured grid gives better accuracy, lower amount of cells and faster convergence compared to unstructured grid. But the grid has to be created using hexahedral blocks, which later are mapped on the surfaces and volumes. This makes it complicated for complex geometries. In contrast, an unstructured grid is faster to generate but for some cases it will lack in quality and have a very large number of cells which increases solution time. For most turbomachinery applications, structured multi-block grids are recommended as it gives a better boundary layer resolution and good control over sharp leading edge and trailing edge of the blades[34].

2.6.2 Turbulence modelling

In CFD the most accurate method is to use DNS(Direct Numerical Simulations), which means the full Navier-Stokes equations are solved for each cell at every time-step. This requires an exceptionally fine mesh to resolve the domain and very small time steps. Using DNS for complex problems still remains unrealistic. So far DNS is used for simple cases at low Reynolds numbers. The next level below DNS simulations is the LES(Large Eddy Simulations), in which the large turbulent scales are resolved and those smaller are modelled using a subgrid-scale model. This leads to a large reduction in use of computational resources

compared to DNS and have sufficient accuracy for many cases. The next are hybrid methods like DES(Detached Eddy Simulations), DDES(Delayed Detached Eddies Simulations) and PANS(Partial Averaged Navier-Stokes), these combine LES with URANS(Unsteady Reynolds Averaged Navier-Stokes). The equations solved in a steady *Reynolds Averaged Navier-Stokes* are displayed in eq 2.24. The additional term in the momentum equations is called Reynolds stress tensor, $\overline{\rho u'_i u'_j}$ and this closure problem is modelled using either Reynolds Stress Models includes non- isotropic effects or eddy viscosity models where turbulence is treated as isotropic[31].

The time averaged continuity equation and Navier-Stokes equation are given as:

$$\frac{\partial \rho}{\partial t} + (\rho \bar{U}_i)_{,i} = 0 \quad (2.23)$$

$$\frac{\partial \rho \bar{U}_i}{\partial t} + (\rho \bar{U}_i \bar{U}_j)_{,j} = -\bar{P}_{,i} + \left[\mu (\bar{U}_{i,j} + \bar{U}_{j,i}) - \overline{\rho u'_i u'_j} \right]_{,j} \quad (2.24)$$

2.6.3 k- ε model

The k- ε model is a two equation model in which the turbulence velocity and length scale are solved using separate transport equations. The velocity scale is resolved from the turbulence kinetic energy, k and the length scale from the turbulent dissipation rate, ε . The k- ε is an eddy viscosity model and is known for its numerical robustness and stability. Hence it is widely used in wide range of industrial applications. The turbulent viscosity used in the k - ε is given as

$$\mu_t = C_\mu \rho \frac{k^2}{\varepsilon} \quad (2.25)$$

The transport of equations for turbulent kinetic energy and turbulent dissipation rate reads as

$$\frac{\partial (\rho k)}{\partial t} + \frac{\partial}{\partial x_j} (\rho U_j k) = \frac{\partial}{\partial x_j} \left[\left(\mu + \frac{\mu_t}{\sigma_k} \right) \frac{\partial k}{\partial x_j} \right] + P_k - \rho \varepsilon + P_{kb} \quad (2.26)$$

$$\frac{\partial (\rho \varepsilon)}{\partial t} + \frac{\partial}{\partial x_j} (\rho U_j \varepsilon) = \frac{\partial}{\partial x_j} \left[\left(\mu + \frac{\mu_t}{\sigma_\varepsilon} \right) \frac{\partial \varepsilon}{\partial x_j} \right] + \frac{\varepsilon}{k} (C_{\varepsilon 1} P_k - C_{\varepsilon 2} \rho \varepsilon + C_{\varepsilon 1} P_{kb}) \quad (2.27)$$

where constants are $C_{\varepsilon 1} = 1.44$, $C_{\varepsilon 2} = 1.92$, $C_\mu = 0.09$, $\sigma_k = 1.0$, $\sigma_\varepsilon = 1.3$. P_{kb} and $P_{\varepsilon b}$ are the buoyancy force influences, P_k is the turbulent production due to viscous forces[33].

2.6.4 Scalable wall functions

Wall functions are the empirical formulas that connects the wall boundary conditions and the solution variable at the near wall grid nodes which is presumed to lie in the fully turbulent region of the boundary layer[33]. The general logarithmic relation is explained earlier in eq 2.13. Scalable wall function in k- ε model is used for the investigations in this report. In scalable wall function, u_τ is replaced by $u^* = C_\mu^{1/4} k^{1/2}$. The frictional velocity is given as

$$u_\tau = \frac{U_t}{\frac{1}{\kappa} \ln(y^*) + C^+} \quad (2.28)$$

The wall shear stress is obtained as

$$\tau_w = \rho u^* u_\tau \quad (2.29)$$

where $y^* = (\rho u^* \Delta y) / \mu$ The main idea of the scalable wall function is to apply a limiter $\bar{y}^* = \max(y^*, 11.06)$ thereby limiting the y^* value not to go below the value of 11.06 thereby all mesh points are outside the viscous sublayer avoiding the fine mesh inconsistencies with wall function approach.

2.7 Wall Roughness Modeling

The prediction of the influence of roughness on the flow aerodynamics and performance of turbomachinery involves developing models that can be used to predict roughness effects on boundary layer growth and transition. The various strategies to implement roughness involves including roughness influence on turbulent eddy viscosity near the wall by usage of modified wall functions, resolving roughness effects on the boundary layer through 'discrete element model'(DEM) and resolving the roughness by DNS.

2.7.1 Roughness modeling in CFX

The wall function used in CFX is formulated based on Launder and Spalding method [33]. Wall roughness is implemented by modifying the law of the wall[33]. The general law of the wall was explained earlier in eq 2.13. Surface roughness on the wall causes a shift in the logarithmic velocity profile which is illustrated in fig 2.5. The modified logarithmic profile reads as

$$u^+ = \frac{1}{\kappa} \ln(y^+) + B - \Delta B \quad (2.30)$$

where $B=5.2$ and the shift, ΔB , is defined as

$$\Delta B = \frac{1}{\kappa} \ln(1 + 0.3k_s^+) \quad (2.31)$$

k_s^+ is the non dimensional roughness height which depends on the equivalent sand roughness height k_s given as

$$k_s^+ = \frac{k_s u_\tau}{\nu} \quad (2.32)$$

k_s is the input variable for ANSYS CFX.

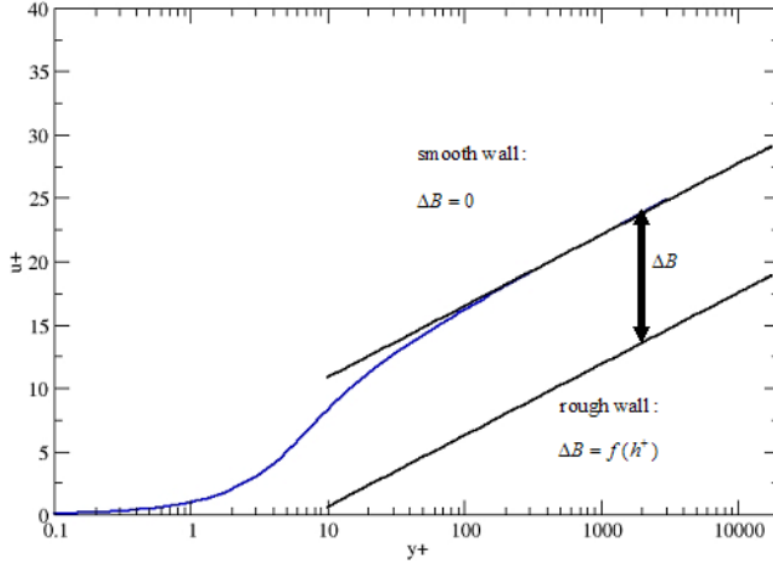


Figure 2.5: *Logarithmic velocity profile with downward shift from ANSYS Manual[33]*

2.7.2 Roughness modeling in Fluent

In Fluent, the law of the wall is modified for including wall roughness effects in wall bounded flows. The modified law of the wall is given as

$$u^+ = \frac{1}{\kappa} \ln(Ey^+) - \Delta C \quad (2.33)$$

where $u^* = C_\mu^{\frac{1}{4}} k^{\frac{1}{2}}$, u_P is the mean velocity at the near wall node P, y_P is the distance from point P to the wall and $E = 9.793$, the empirical constant. The function ΔC is depending on k_s^+ and C_s which is a roughness constant. The value of C_s depends on the type of roughness. The three different regimes are shown in table 2.4

An example of the influence of different roughness sizes on the velocity profile is shown in fig 2.6. The roughness on the wall induces a shift in velocity profile near the wall. This is shown in the fig 2.6 where the downward shift in the log layer of the velocity profile is clearly pronounced with increase in roughness sizes from $1 \mu\text{m}$ to $25 \mu\text{m}$.

Table 2.4: Fluent: Roughness regimes based on dimensionless roughness parameter

hydraulically smooth	$k_s^+ \leq 2.25$	$\Delta C = 0$
transition region	$2.25 < k_s^+ \leq 90$	$\Delta C = \frac{1}{\kappa} \ln \left[\frac{k_s^+ - 2.25}{87.75} + C_s k_s^+ \right] * \sin(0.4258(\ln k_s^+ - 0.811))$
fully rough	$k_s^+ > 90$	$\Delta C = \frac{1}{\kappa} \ln(1 + C_s k_s^+)$

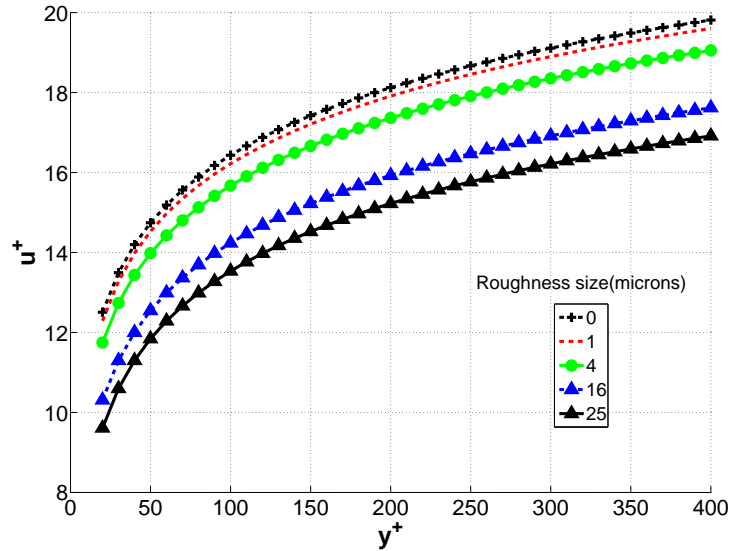


Figure 2.6: Roughness shift in near wall velocity profile in CFX

2.8 Limitations in CFD involving turbomachinery

CFD has been served as a valuable tool in the design and optimization of turbomachinery for many years. As CFD involves approximations of the real flow, it is not advisable to rely completely on the values from CFD and proceed further for production. Even though there are many recent developments in CFD, it cannot completely replace experiments and rig tests. As Denton[24] says 'CFD should be used on a comparative basis and not trusted to give quantitative predictions of performance'. CFD predictions involve different sources of error which affects the accuracy of the calculations. The various error sources are numerical errors, modeling errors, unknown boundary condition and unknown geometry. Numerical errors are caused due to the approximations used in the numerical methods and stabilising factors involved in the CFD code. This is usually reduced by using finer grids. Modeling errors arise from modeling of turbulence, transition, tip leakage modeling and mixing planes which are introduced for steady flow predictions through blade rows in relative motion. Unknown boundary conditions includes defining end wall boundary layer and free stream turbulence level at the inlet. As different boundary conditions affects the predicted performance. Unknown geometry error consists of example deviations of blade profiles from the intended geometry, fillets, tip clearances and surface roughness. Another demanding part in using CFD is the estimation of stalling point for a compressor. In general, the stall point can be taken as the highest total pressure ratio or the point when the mass flow decreases with more iterations known as numerical stall. Stall can be triggered due to various causes. Example of a stall mechanism is rotating stall. It is often recommended to keep in mind the limitations of CFD while predicting trends and it is valuable tool for evaluation of turbomachinery components.

Chapter 3

Numerical study of an airfoil

3.1 Numerical 2D Simulations

The 2D simulations involves the numerical analysis of a NACA 0012 airfoil with surface roughness and validating the simulations with experimental results obtained from a NACA report[14]. The numerical analysis included generation of the computational grid, setting up and running the simulation and then postprocessing of the results. The RANS steady simulations were carried out in ANSYS CFX and ANSYS FLUENT. The wall surface roughness models were enabled for simulations in both the packages and comparisons were done for the aerodynamic characteristics of the airfoil. The main notion behind the 2D simulations was to validate the wall roughness models in different packages which will be used for 3D simulations of a transonic compressor stage.

3.1.1 Geometry and mesh generation

The 2D computational domain for the airfoil was created in ICEMCFD by importing the airfoil coordinates for a NACA 0012 airfoil. The inlet was placed at a distance of 15 times the chord length from the leading edge and the outlet at a distance of 10 times the chord length from the leading edge. A structured C-type block mesh was created around the computational domain. An average y^+ value of 30 was maintained for the first layer height from the wall to incorporate wall functions in the simulations as required for roughness modeling. The usage of wall functions helps in the reduction of the computational mesh which in turn reduces the expense of computational resources compared to usage of low-Reynolds number models or LES models. The computational domain and the mesh is shown below in the figures 3.1a and 3.1b.

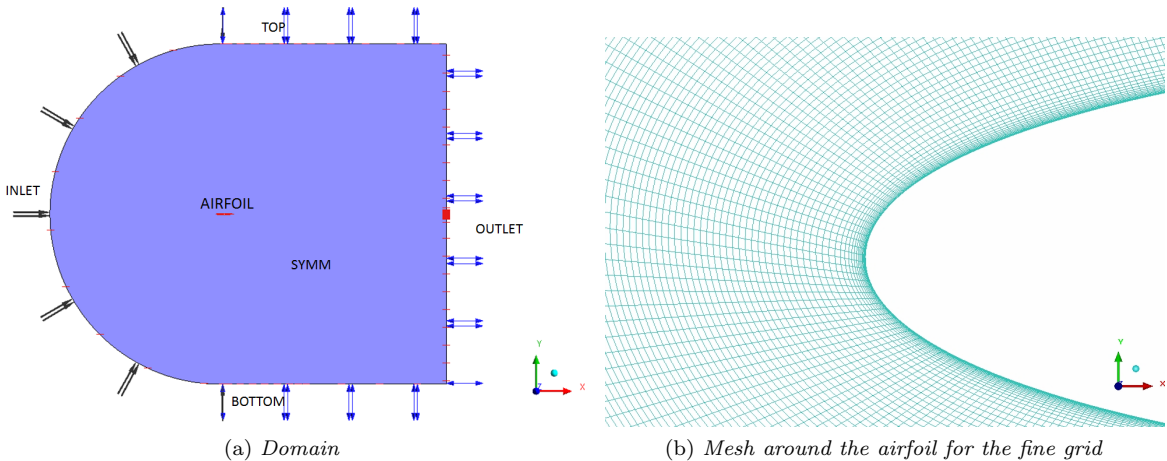
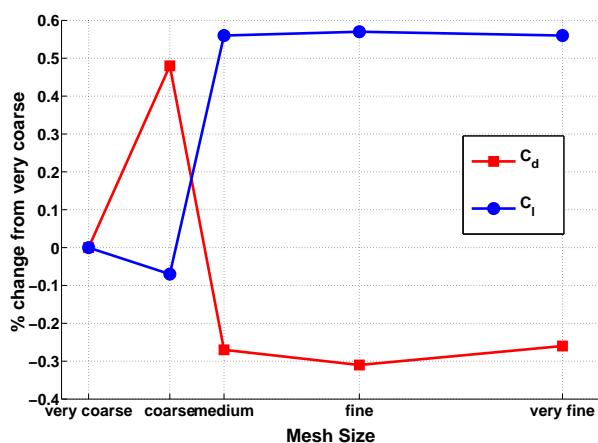


Figure 3.1: *Computational domain*

A mesh independence study was done for the computational domain to reach convergence of variables with respect to the mesh resolution. This study was done to remove the uncertainties due to change in number of cells in the grid. The grid for the airfoil domain was generated with the following cell counts: very coarse, coarse, medium, fine and very fine. The medium mesh was chosen as there is negligible difference in value of aerodynamic parameters with further increase in density of mesh as shown in fig 3.2. The figure shows the deviation of C_l and C_d for the airfoil at 0° angle of attack from that for the coarse mesh.

Figure 3.2: *Mesh convergence*

3.1.2 Boundary conditions

The simulation boundary conditions for Fluent were set-up as in table 3.1, with uniform inlet velocity $v = 62$ m/s. The velocity was calculated using the Reynolds number used in the NACA experiment was 3,100,000 with which results are to be compared.

Table 3.1: ANSYS Fluent Boundary conditions, $v =$ inlet velocity

Boundary type	Boundary condition	Values
Inlet	Pressure Far-Field	Mach number = 0.1787 Gauge Pressure = 101325 Pa Temperature = 300K Turbulent intensity = 1% Turbulent viscosity ratio = 1
Outlet	Pressure Outlet	Gauge Pressure = 101325 Temperature = 302K
Airfoil	Wall	$v = 0$
Top	Pressure Far-Field	Mach number = 0.1787 Gauge Pressure = 101325 Pa Temperature = 300K Turbulent intensity = 1% Turbulent viscosity ratio = 1
Bottom	Pressure Far-Field	Mach number = 0.1787 Gauge Pressure = 101325 Pa Temperature = 300K Turbulent intensity = 1% Turbulent viscosity ratio = 1

The boundary conditions for ANSYS CFX simulations are given in the table 3.2

Table 3.2: ANSYS CFX Boundary conditions

Boundary type	Boundary condition	Values
Inlet	Inlet	Velocity = 62 m/s given as Cartesian Components Static Temperature=300K Temperature = 300K Turbulent intensity = 1%
Outlet	Opening	Entrainment , Pressure=101325 Pa Turbulence = Zero Gradient Static Temperature = 302K
Airfoil	Wall	$U = 0$
Top	Opening	Entrainment , Pressure = 101325 Pa Turbulence = Zero Gradient Static Temperature = 302K
Bottom	Opening	Entrainment , Pressure = 101325 Pa Turbulence = Zero Gradient Static Temperature = 302K
Symmetry	Symmetry	-

3.1.3 Simulations

The simulations were carried out using ANSYS CFX and ANSYS FLUENT commercial solver packages. A compressible, implicit solver was used in both ANSYS CFX and ANSYS FLUENT cases. The turbulence model chosen was $k-\varepsilon$ with scalable wall function as it is robust and applied in vast fields of this application. In both the solvers, the roughness was introduced on the wall by specifying uniform sand grain roughness height. From the experimental data [14], surface irregularity from the machine cut finish was given as 0.0005 inches in depth. This was otherwise called technical roughness which was the result of the manufacturing processes. The equivalent sand grain roughness for the given technical roughness was calculated using the empirical relations described in table 2.3. The peak to valley value of surface roughness was used for the conversion to equivalent sand grain roughness due to the type of surface roughness specified in the NACA report [14]. In Fluent, in addition to roughness height, a roughness constant was needed to be specified, The range of the value was 0.5-1.0 and this value depends on the type of roughness. For uniform roughness, the default value of 0.5 was chosen and it was also recommended for $k-\varepsilon$ turbulence model[33].

The simulations were carried for different angle of attacks ranging from $\alpha = 0^\circ$ to $\alpha=12^\circ$. The convergence criteria for the residuals achieved were in the order of $10e-05$ stable residuals and constant value of aerodynamic coefficients with more iterations. The aerodynamic coefficients C_l and C_d was calculated for the whole range of angle of attack. The aerodynamic coefficients were compared with the experimental data from NACA report [14].

3.2 Results and Validation

The results of the 2D analysis of the NACA airfoil with surface roughness in comparison with the experimental data [14] is discussed here. The predictions of the aerodynamic coefficients C_l and C_d for the NACA 0012 airfoil smooth and rough wall cases are shown in the fig 3.3 and 3.4. It can seen from the fig 3.3 that there is no significant change in C_l values due to roughness. This can be explained as lift is due to pressure difference between the upper and lower surface of the airfoil and it is less influenced by the roughness on the surface compared to drag component. This argument is also supported by the static pressure distribution on the airfoil shown at $\alpha = 0^\circ$ and $\alpha = 9^\circ$ in fig 3.7 and fig 3.8 respectively. This also prevails even at higher angles of attack.

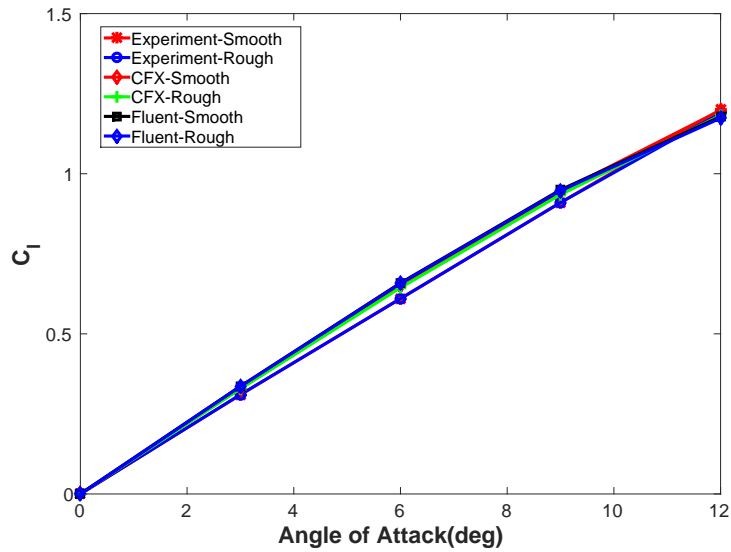


Figure 3.3: C_l Vs Angle of attack

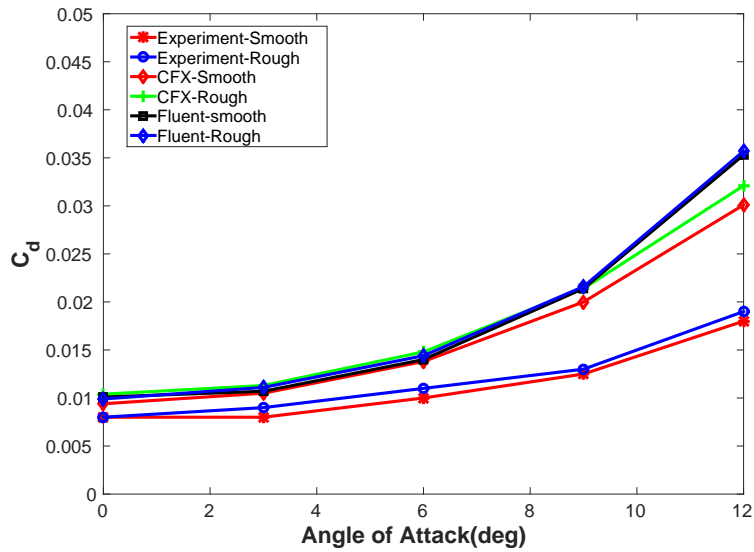


Figure 3.4: C_d Vs Angle of attack

From the fig 3.4, the disagreement of C_d values with respect to the experimental data is seen and it is more pronounced at higher angles of attack. The over-prediction of drag could be due to the high wall shear stress prediction in use of standard turbulence model[1]. The wall shear stress and static pressure variation along the airfoil at 0° and 9° for ANSYS CFX and ANSYS FLUENT results are shown in figures 3.5 - 3.8. From the fig 3.5 and 3.6 it can be seen that wall shear stress is increased for the rough airfoil compared to the smooth airfoil. This shows that roughness influences the viscous force in contrast to the pressure force resulting in increase in drag values for the rough case.

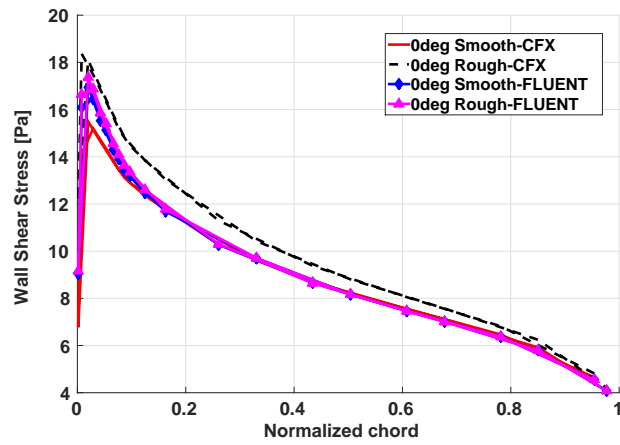


Figure 3.5: Wall shear stress at $AOA=0^\circ$

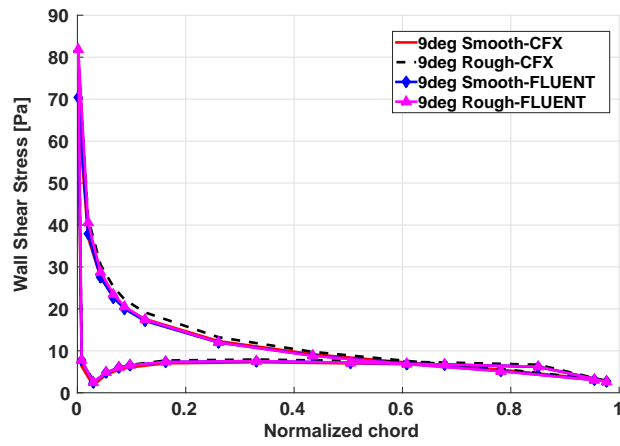


Figure 3.6: Wall shear stress at $AOA=9^\circ$

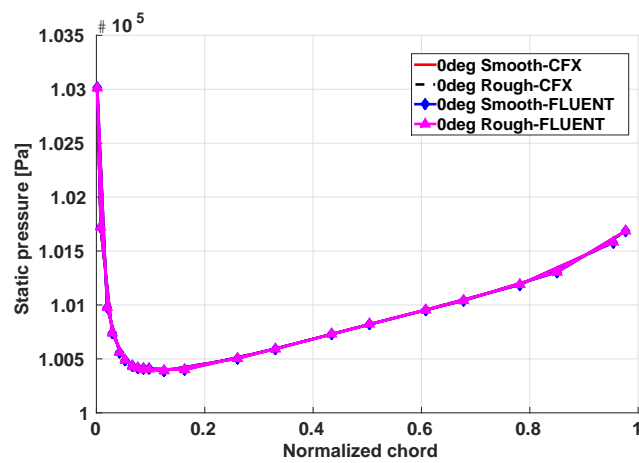
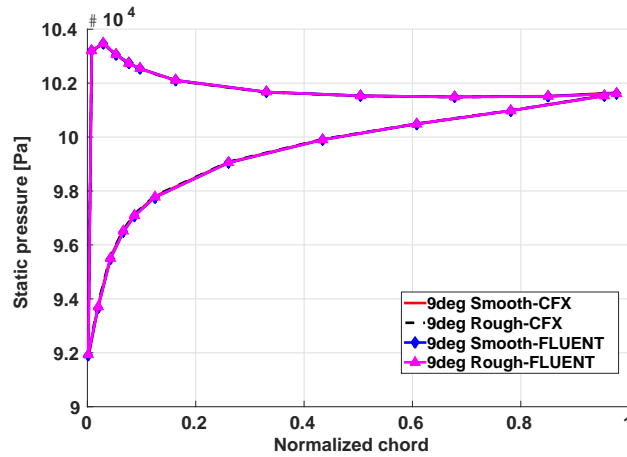
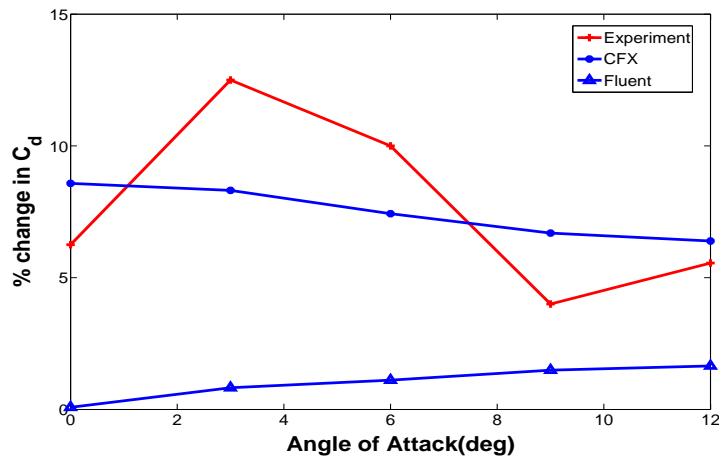


Figure 3.7: Static pressure at $AOA=0^\circ$


 Figure 3.8: *Static Pressure at AOA=9°*

The results for the drag coefficient from ANSYS CFX simulations and ANSYS Fluent are compared with the experimental data in terms of increase in C_d (in %) value due to roughness compared with the smooth case. The % change in C_d values for ANSYS CFX and ANSYS Fluent are shown in fig 3.9 with reference to experimental data. The ANSYS CFX data shows better agreement with the experimental data than compared with the ANSYS Fluent data. This could be due to the difference in shear stress predictions of the turbulence model for separating flows with the effect of roughness included[1]. Hence ANSYS CFX roughness modeling was used for the simulations of the transonic compressor stage.


 Figure 3.9: *Change in C_d from smooth to rough surface*

3.3 Transition simulations

The effect of transition on the aerodynamic coefficients of the airfoil was investigated by enabling the transition modeling in ANSYS CFX. Simulations were done using the built-in transition model formulation, Gamma-Theta transition model developed with SST turbulence model in ANSYS CFX. The figure 3.10 and 3.11 shows the C_l and C_d variation with angle of attack comparing the steady state simulations for the NACA airfoil with and without transition. The transition simulations were done for smooth case and rough case where the rough case is done for equivalent sandgrain roughness size, $12\mu\text{m}$ as used in the report. The mesh used for transition simulations is low-Reynolds grid with y^+ value of 1. The influence of transition on C_l shows agreement with experimental values compared to without transition. Transition modeling shows insignificant change in drag prediction at higher angle of attack compared to without transition but at lower angle of attack it gives

under-prediction of drag values. This can be due to the assumption of fully turbulent over the airfoil in turbulence modeling and also it emphasizes the need for providing proper transition point between laminar to turbulent flow over the airfoil.

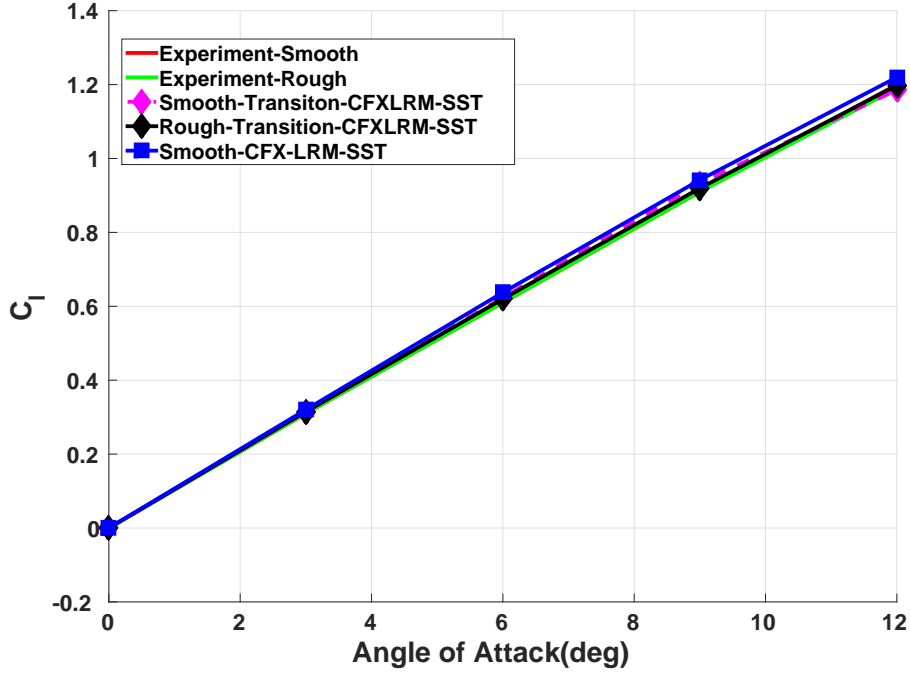


Figure 3.10: *Lift curve from the transition simulations*

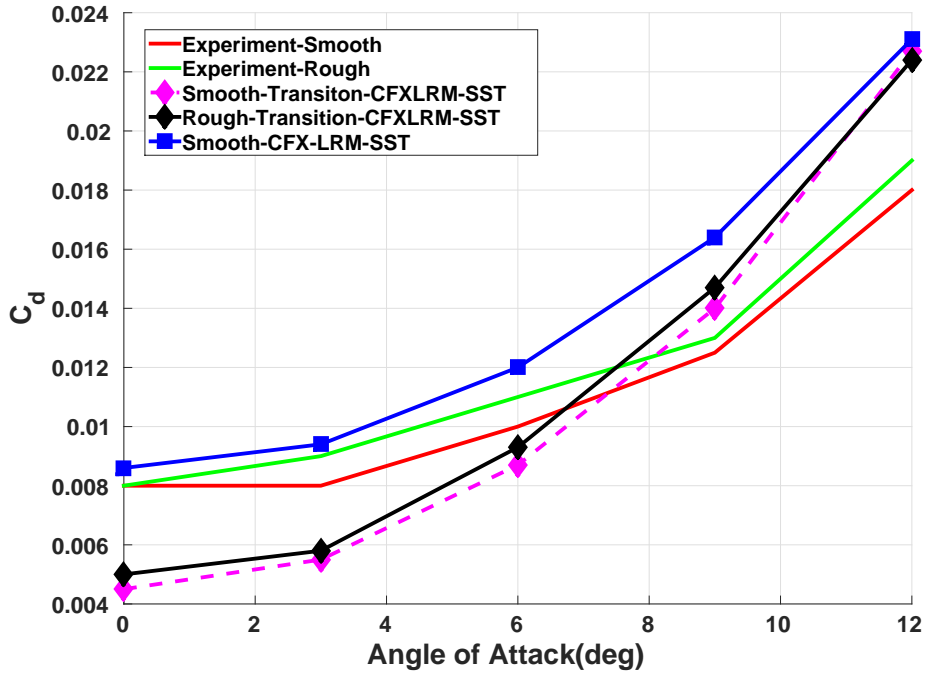


Figure 3.11: *Drag curve from the transition simulations*

Chapter 4

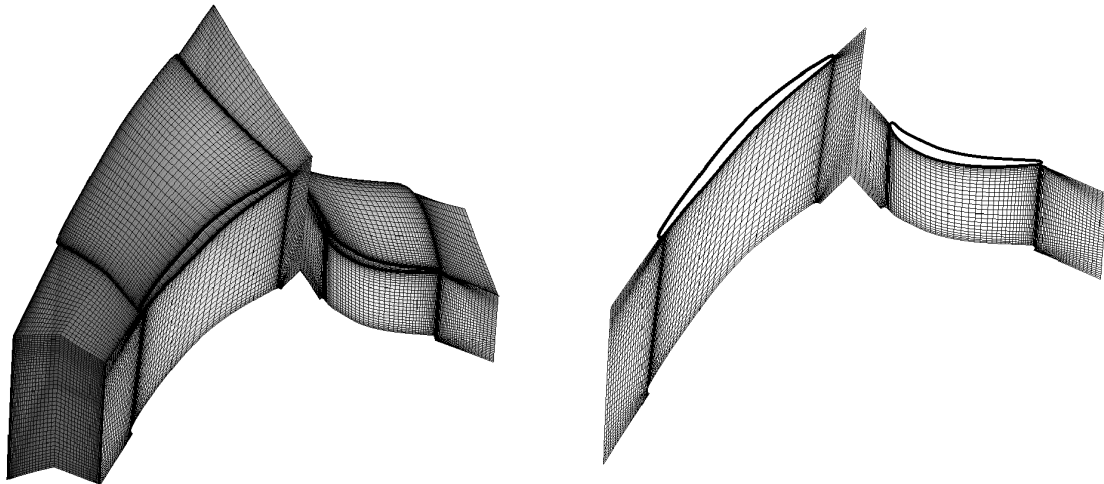
Numerical study of a compressor stage

4.1 3D Stage Simulations

The 3D simulations were carried out for a research compressor stage consisting of a rotor and a stator. RANS calculations were done for the stage domain using the commercial CFD solver ANSYS CFX and the results were analysed in CFX-Post.

4.1.1 Geometry and grid generation

The stage geometry consists of a rotor blade and a stator blade along with hub and shroud. The flow enters the rotor domain from a plenum. A structured multi-block mesh was created for the stage domain. The blade geometry was fitted with O-grid to resolve the boundary layer around the blades. The blade passages and the inlet and outlet passages were controlled by H-grid blocks. An average y^+ value of 30 was maintained over the grid for the use of wall functions for the surface roughness study. The mesh for the domain and a section view for the mesh in mid span were shown in the fig 4.1a and fig.4.1b.



(a) Mesh around rotor and stator

(b) Mesh in blade-to-blade section

Figure 4.1: Computational Mesh of the domain

4.1.2 Boundary Conditions

The computational domain for the stage model is illustrated in fig 4.2. The flow enters the rotor from a plenum which was employed to specify the inlet variables in an absolute frame of reference. The inlet condition was specified with radial profile values for k , ε , T_0 , P_0 and velocity components. An opening boundary condition with specified static pressure was used at the outlet. The rotor domain was set to rotating and for other domains were set to stationary. An adiabatic no slip condition was used for the wall surfaces which includes blades, hub and shroud. The rough wall condition with specified sand grain roughness height was used for the rough cases. A range of sand grain roughness heights were used for the simulations which represented the roughness from a standard manufacturing process. Only one blade passage was resolved with periodic

boundary condition. A general connection interface model with stage option was used for the interface between the rotating domain and the stationary domain. The stage boundary condition is a mixing plane interface which is the commonly used condition when there exists a frame change between the rotor and the stator in steady state simulations. The idea behind this stage interface model is that at the interface a circumferential averaging of the fluxes is done between the rotating passage and stationary passage on the two sides of the interface[5]. The interface model ensured the steady state solutions for multi-stage calculations. The change in pitch between the rotor and stator was specified by pitch angles at the stage interface. This stage model also induce a one time mixing loss.

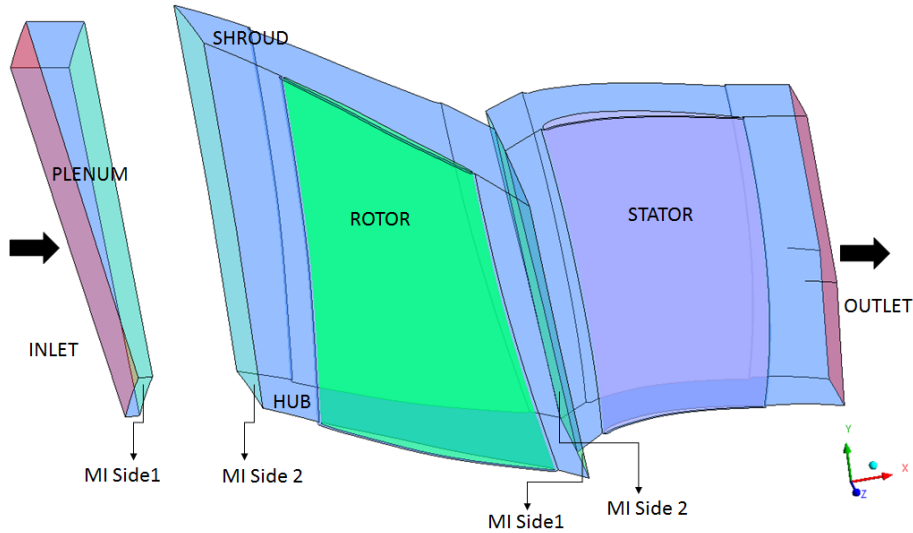


Figure 4.2: *Computational Domain with Mixing plane Interfaces(MI)*

4.1.3 Simulations

Steady RANS simulations were carried out for a transonic compressor stage in ANSYS CFX. The simulations were done for smooth surfaces and rough surfaces. The cases were compared along a throttle line generated for a constant throttle area. This was because, if pressure ratio was taken for reference for comparing the different roughness sizes along a speedline on the compressor map, it might fall near the stall region and when considering mass flow for reference this will fall near the choking point for the working speed line which is illustrated in fig 4.3. Hence to remove this complication, all the simulations were calculated along the same working line to give a good comparison between the cases. The throttle area corresponding to the operating points were obtained by using equation 2.9 and were monitored while performing simulations. The prediction of stall point is a major concern in the turbomachinery CFD. The numerical stall point however approximate as the mass flow when approaching stall will decrease slowly with increasing iterations[4]. Hence the predictions were confined to the one operating point which is the design point for 100% rotation speed. The design point was obtained by performing smooth case simulations which corresponds to smooth wall condition for different operating points along the speed line. The turbulence in the simulating domain was modelled by choosing $k-\varepsilon$ turbulence model with scalable wall functions as discussed in section 2.6.3. The postprocessing of the results were done in ANSYS CFX-Post and MATLAB. The radial variation of the flow properties were obtained by circumferential averaging by taking sampling points distributed along hub to shroud path with equal mass flow over circular bands concentric about the rotation axis which is shown in fig.4.4. The separations over the blades were shown by the surface streamlines on the surfaces. The variation of flow variables near the wall were also analysed for the effect of roughness on the surfaces.

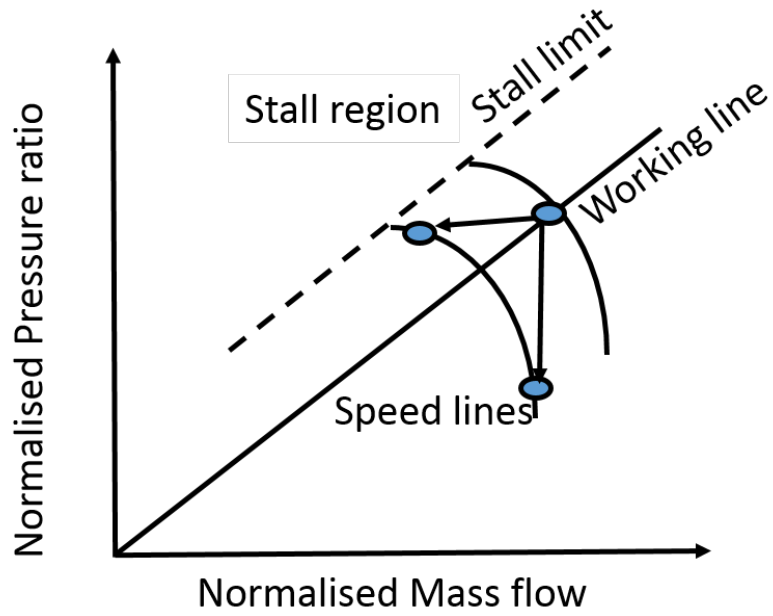


Figure 4.3: *Design point representation*

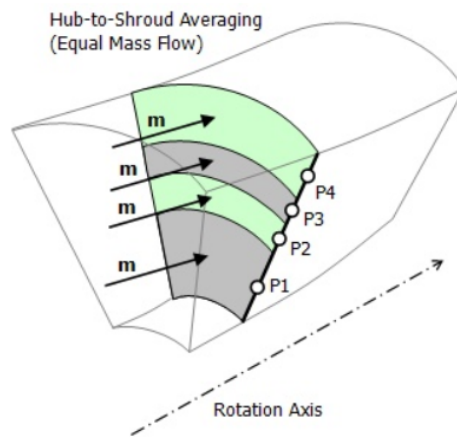


Figure 4.4: *Circumferential averaging of flow variables - Fig from ANSYS manual[33]*

4.1.4 Mesh Independency study

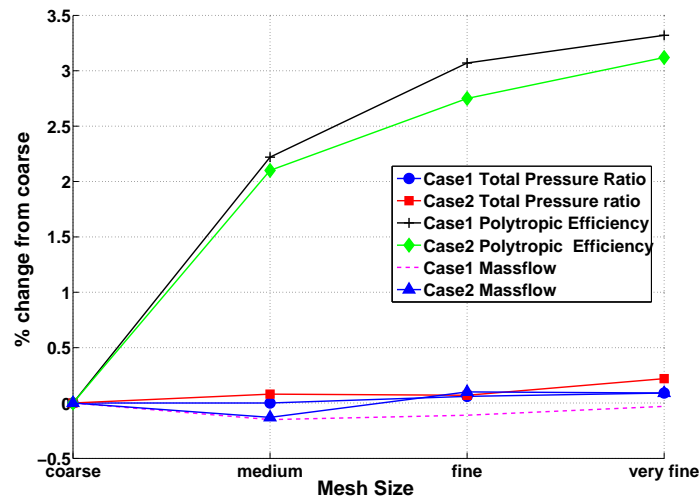
A mesh independency study was done to check the dependency of the mesh on the convergence of the solution variables. The different sizes of the grid are shown in the table 4.1. The different grids were obtained by increasing and decreasing the number of grid points in each coordinate direction. The simulations were carried out for the above mentioned grids to calculate the performance parameters of the transonic compressor stage. The sensitivity study was done for three cases, smooth, roughness only on the rotor blade and roughness in rotor and stator blades. The roughness size considered for mesh study was $25\mu m$. The simulations were carried out for the design point along the working line generated using a constant throttle area. The variations in the flow parameters mass flow, total pressure ratio and polytropic efficiency with respect to grids were shown in fig 4.5. The percentage change in the performance values compared with the coarse mesh was evaluated for two cases, case 1: smooth case and case 2: roughness in stator and rotor blades. The change in efficiency was more pronounced compared to the changes in other performance parameters. The change in values were below 0.5% after the fine mesh which has taken as criteria to select the mesh for further study. Based on the results from the mesh independency study, the fine mesh was taken for further analysis of the stage with different roughness sizes. The simulations with fine mesh for the further analysis of the stage were done in a cluster environment provided by Chalmers Centre for Computational Science and Engineering, Göteborg.

Table 4.1: Grids used for mesh independency study

Mesh	Number of elements
Coarse	20608
Medium	127744
Fine	372480
Very fine	621056

Table 4.2: Investigated sand grain roughness sizes[35]

Type of cause	Sand grain roughness, k_s
Fouling & Manufacturing	$1\mu m$
	$2\mu m$
	$4\mu m$
	$8\mu m$
Erosion	$16\mu m$
	$20\mu m$
	$25\mu m$

Figure 4.5: *Mesh independency convergence*

4.2 Stage simulation results

The CFD predictions of the compressor stage performance characteristics and the flow field characteristics of the stage domain are presented in this section. The predicted compressor performance with and without surface roughness cases can be seen in figures 4.6 - 4.7 compared along a throttle line generated using a constant throttle area. Two rough cases under investigation are denoted as R for roughness in rotor blade and SR for roughness in rotor and stator blades. The sand grain roughness sizes k_s of $1\mu\text{m}$, $2\mu\text{m}$, $4\mu\text{m}$, $8\mu\text{m}$, $16\mu\text{m}$, $20\mu\text{m}$ and $25\mu\text{m}$ listed in table 4.2 which categorizes into fouling and erosion [35] are used for evaluation of the effect of roughness. The total pressure ratio, polytropic efficiency and corrected mass flow presented are normalised with their respective values from the smooth case. The performance degradation due to roughness in compressor stage has been previously reported by Gbadebo et al [12], Bammert et al [6], Syverud et al [18] and Kang et al [19] both numerically and experimentally. The results of total pressure ratio variation with corrected mass flow for the compressor stage performance map are shown in fig 4.6. The operating point for the smooth surface was taken as the reference point for comparison. The working line for the operating point was calculated and plotted which is shown as solid line in fig 4.6. The total pressure ratio and mass flow decreases as the roughness increased on the blade surface. This is the same trend as shown in the results by Syverud et al [18]. As it was seen in the polytropic efficiency drop, there is increased loss in total pressure ratio and mass flow in the SR case compared to R case. Compared to smooth and highest roughness size, the total pressure ratio decreased by 0.5 % and corrected mass flow by 0.8%.

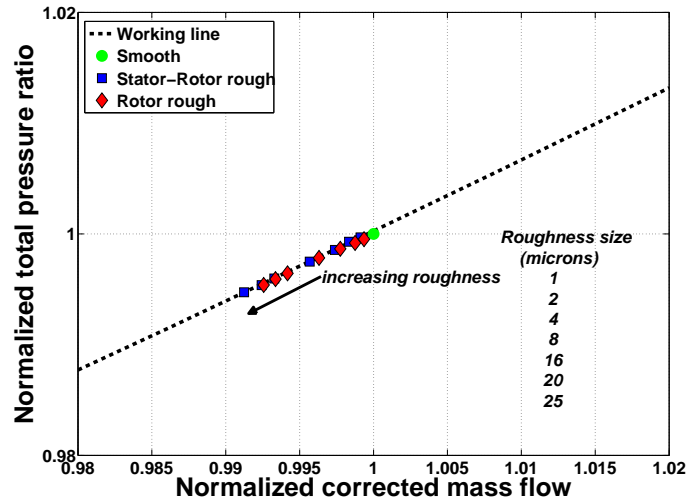


Figure 4.6: *Compressor map from the simulations at design point*

It can be seen from the fig 4.7, there is a significant drop in polytropic efficiency with increase in roughness for both rough cases compared to the smooth case. The drop in the polytropic efficiency from smooth to maximum roughness of $k_s = 25\mu\text{m}$ accounts for 2.6% in SR case and 2.0% in R case. The drop in efficiency in reference to smooth case is more affected by the roughness on rotor blades than adding roughness on stator blades. The general trend of polytropic efficiency decline due to roughness was reported in Woelk et al [6]. The drop in corrected mass flow and total pressure ratio are shown in fig 4.8a and 4.8b respectively.

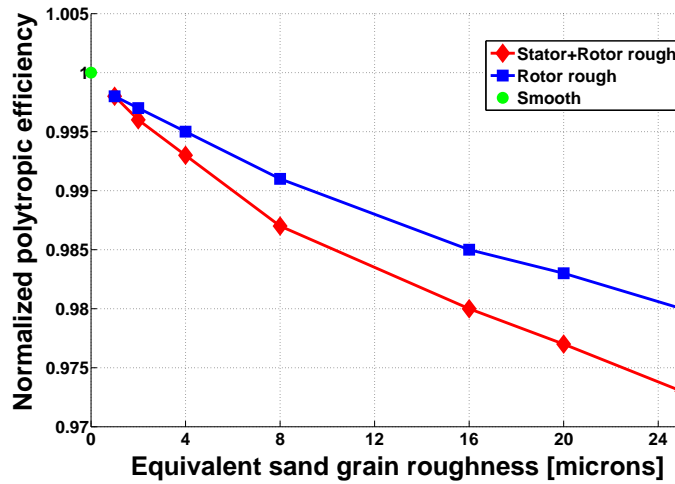


Figure 4.7: *Polytropic efficiency for the compressor stage*

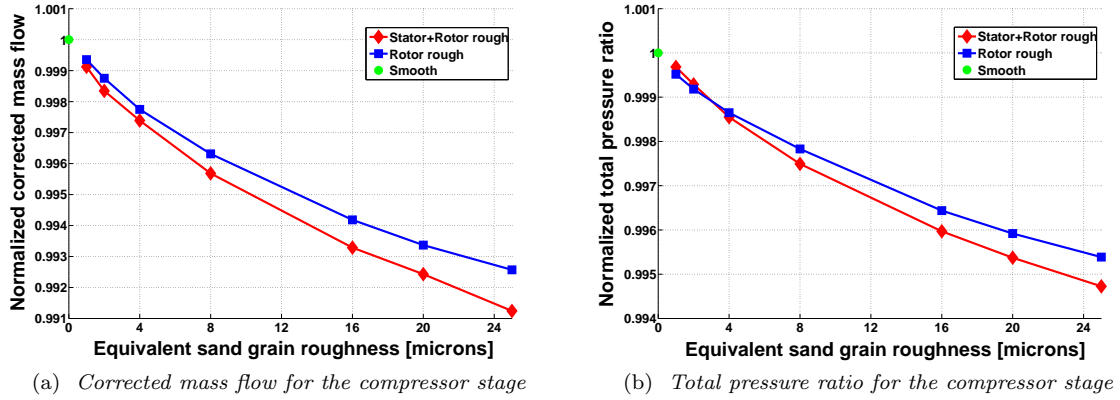


Figure 4.8: Performance of the stage

Radial distributions of relative total pressure in the rotor and stator domain are presented in fig. 4.9 and fig. 4.10 respectively. The radial profiles were extracted at the leading edge and trailing edge of the rotor and stator blade surfaces. The reduction in relative total pressure is shown for the rough case compared to the smooth case in fig 4.9a and fig. 4.9b. There is a reduction in decline of total pressure near the hub corner region of the rotor trailing edge with the roughness on the surfaces. This same trend is seen at the leading edge and trailing edge of the stator in the fig. 4.10a and fig. 4.10b. In contrast to rotor, the effect of roughness on the stator blade total pressure is seen for both leading and trailing edge as the flow is disturbed by the rotor roughness before it enters the stator. At the trailing edge of the stator blade, addition of roughness has caused a larger loss in total pressure in the stator + rotor rough (SR) case compared to the rotor rough case.

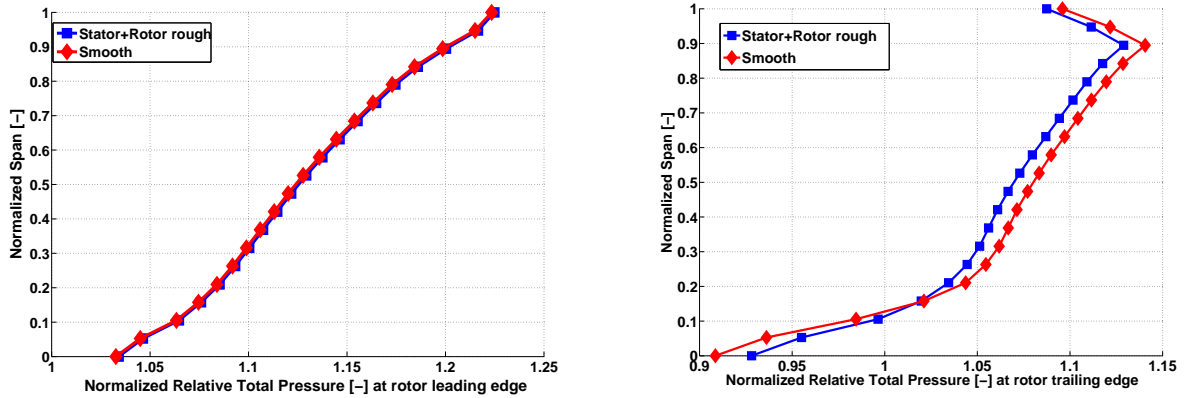
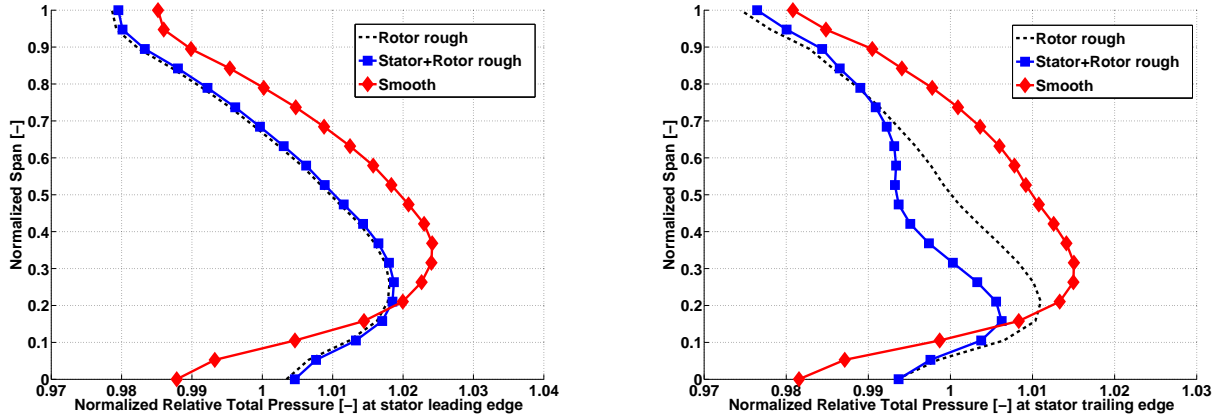


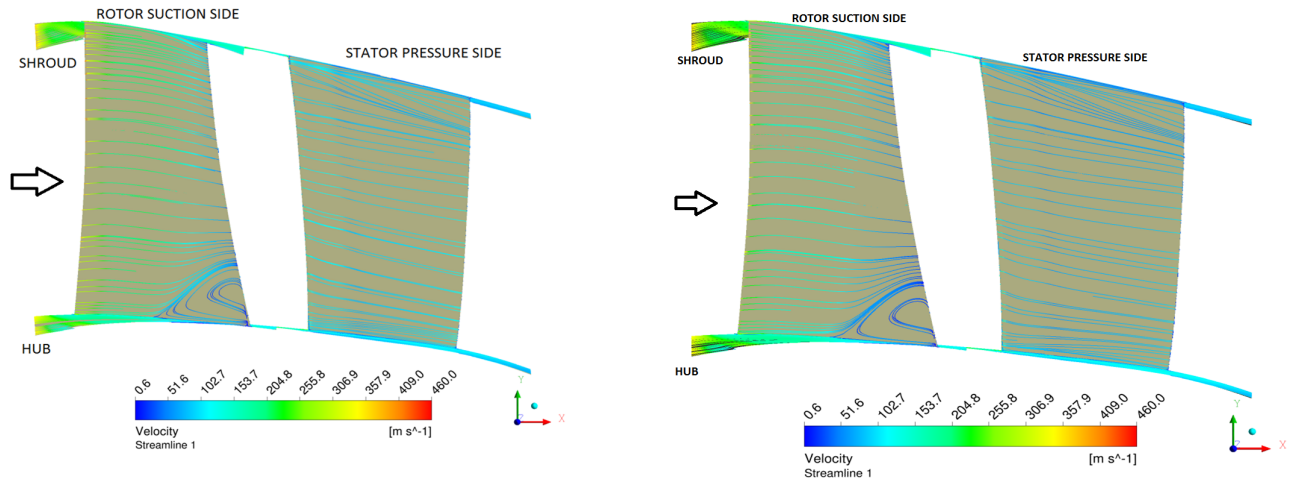
Figure 4.9: Spanwise plot for Rotor blade



(a) Spanwise relative total pressure distribution at stator leading edge (b) Spanwise relative total pressure distribution at stator trailing edge

Figure 4.10: Spanwise plot for Stator blade

The streamlines of velocity just outside the boundary layer over both sides of the rotor and stator blades are presented in fig. 4.11a-fig. 4.11b and fig. 4.12a-fig. 4.12b. This plots shows an overview of the flow field over the blades. The plots are shown for the maximum roughness size $k_s = 25\mu\text{m}$. The separation near the hub region of the rotor trailing edge can be seen in fig. 4.11a for the smooth surface and in fig. 4.11b for the rough surface. The rotor suction side trailing edge is more influenced by the increase of surface roughness than the leading edge. From the fig. 4.12b it can be inferred that the roughness in stator blades has caused separation on the suction side of the stator blade near mid span region. As it mentioned in other research from Chen et al [16], the pressure side of the blades are less affected by the surface roughness compared to the suction side.

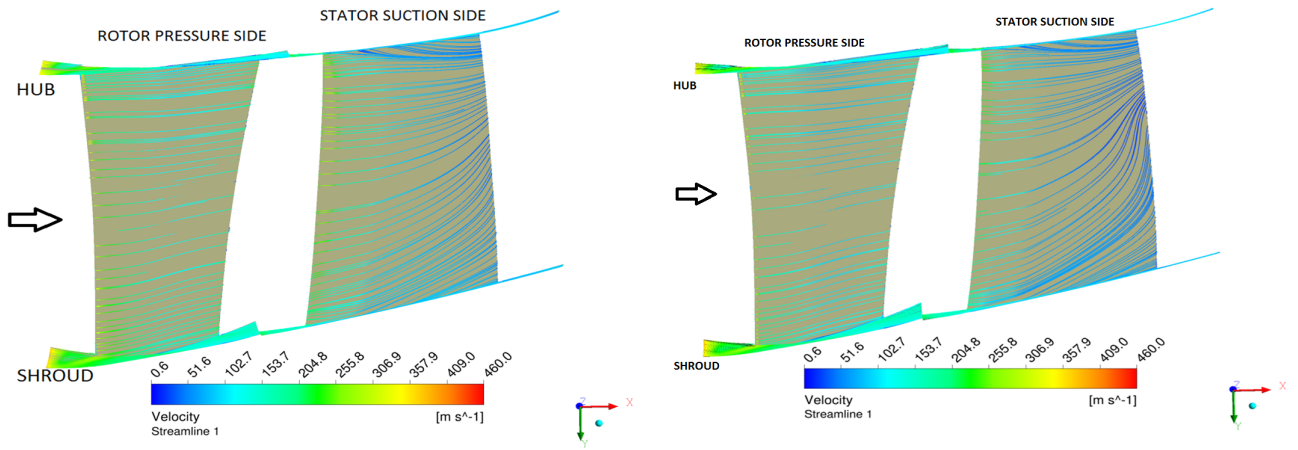


(a) Velocity for smooth case

(b) Velocity for stator and rotor rough case

Figure 4.11: Surface streamline contours on suction side of rotor and pressure side of stator

In order to investigate further the separation and relative total pressure loss near the trailing edges of rotor and stator, the contours of relative total pressure are shown at the rotor exit and stator exit planes. The fig. 4.13a & fig. 4.13b shows the relative total pressure contours for the smooth and stator + rotor rough (SR) case. The contours are shown from hub to shroud correspondingly from bottom to top in the figures. The roughness case shown here is for highest roughness size of $25\mu\text{m}$. It is shown that a thicker wake region is formed from the hub region to mid span region of the blades with addition of roughness on the blade surface compared to the smooth case in fig. 4.13b. It is also shown that there is some reduction in total pressure loss

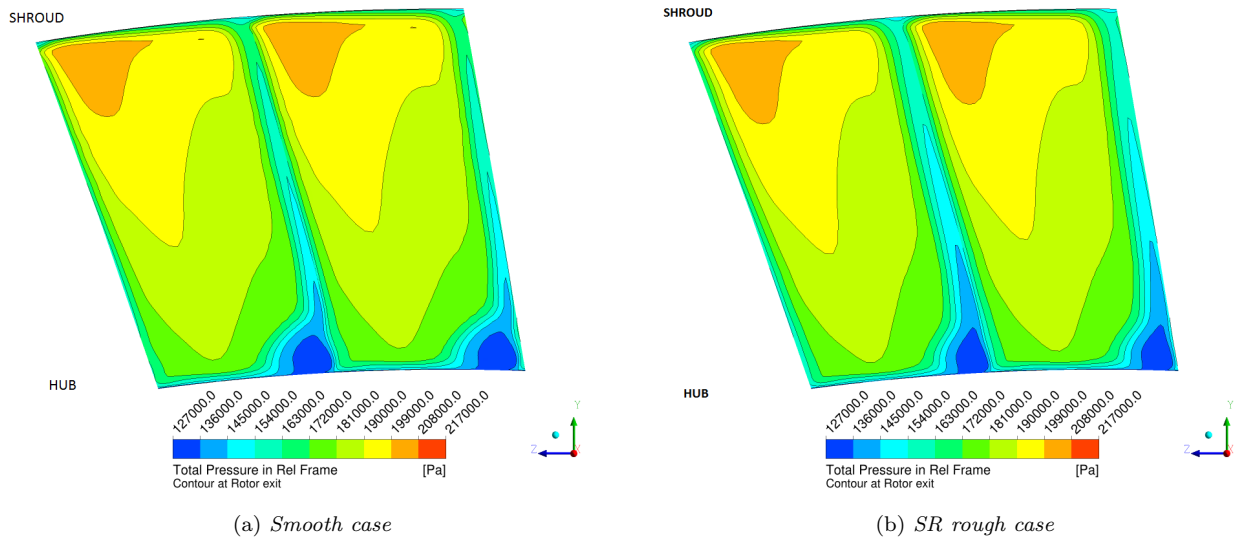


(a) Velocity for smooth case

(b) Velocity for stator and rotor rough case

Figure 4.12: Surface streamline contours on pressure side of rotor and suction side of stator

near the hub region at the rotor trailing edge due to the influence of roughness in section 4.2. The contours of total pressure for smooth case and rough cases at the stator exit are shown in the fig. 4.14a - fig. 4.14b. The increase in wake is shown in the mid span region of the stator blades in fig. 4.14b.

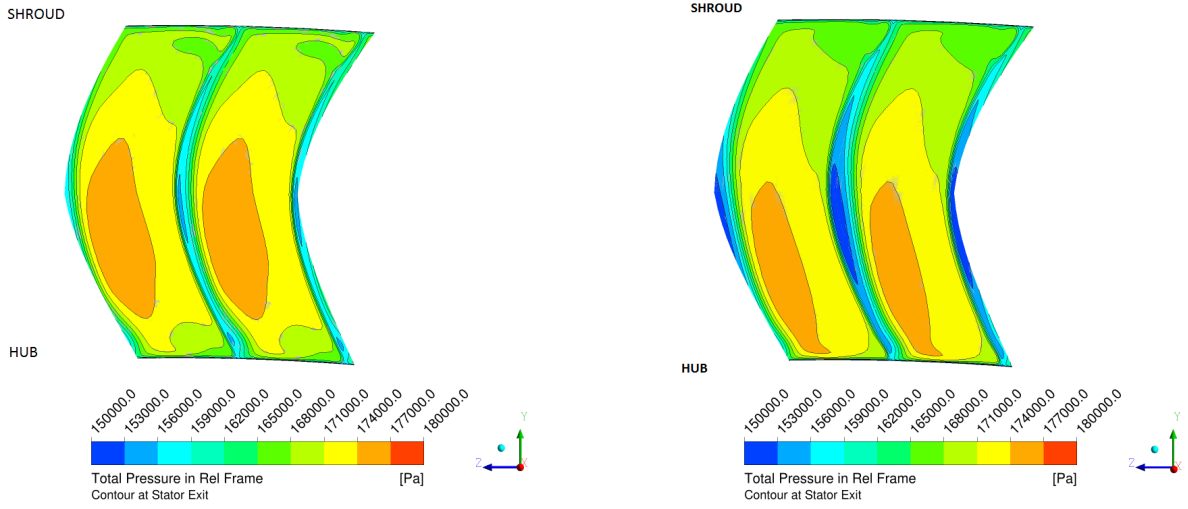


(a) Smooth case

(b) SR rough case

Figure 4.13: Relative Total Pressure contours at the exit of the rotor

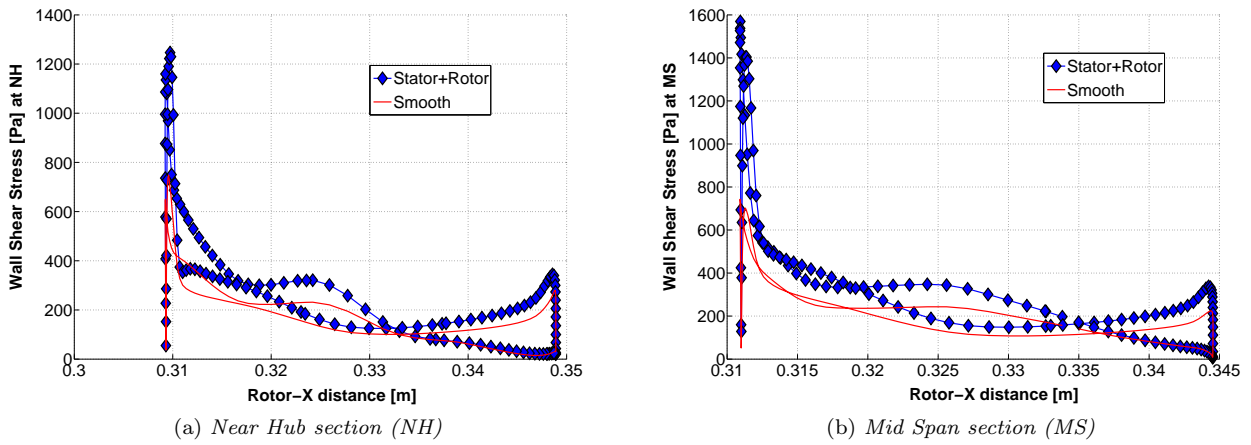
The effect of roughness on wall shear stress over the blades is analysed for the different spanwise section of the blades. Three regions are analysed which are near hub section corresponds to 10% of span, mid span section corresponds to 50% of span and near tip section corresponding to 90% of span. The increase in wall shear stress with roughness introduced over the rotor blades are shown in fig. 4.15a - fig. 4.15c which shows the characteristic increase in skin friction due to roughness on the blade surfaces.



(a) Smooth case

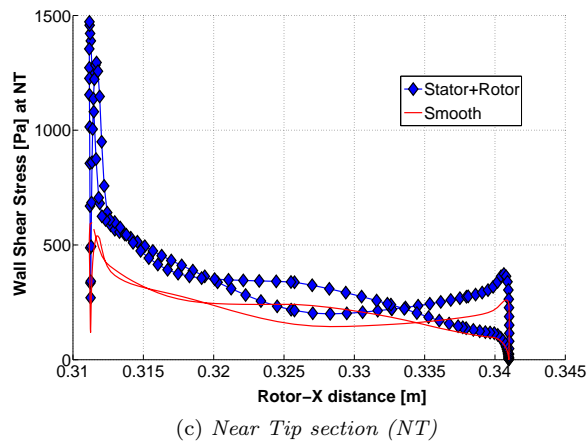
(b) SR rough case

Figure 4.14: Relative Total Pressure contours at the exit of the stator



(a) Near Hub section (NH)

(b) Mid Span section (MS)



(c) Near Tip section (NT)

Figure 4.15: Wall shear stress at different span sections of rotor

4.3 Roughness over hub and shroud region

Having analysed the roughness on the rotor blade showing separation reduction at the near hub region, simulations were done by including roughness on all the surfaces which includes rotor and stator blades, hub and shroud surface. The analysis was done for the maximum roughness size $25\mu\text{m}$. The radial distribution of the relative total pressure at the rotor and stator blades are shown in fig 4.16a - 4.17b. Roughness effects were more pronounced near the trailing edge region compared to leading edge region for the rotor and stator blades. The fig 4.16b and 4.17b shows the relative total pressure variation at the trailing edge region of rotor and stator respectively. It showed loss in relative total pressure at the trailing edge of the rotor and stator blades at the hub and tip region. This conveys the fact that the separation near the hub region and wake near the mid span and the tip region is further increased with the roughness in hub and shroud surface.

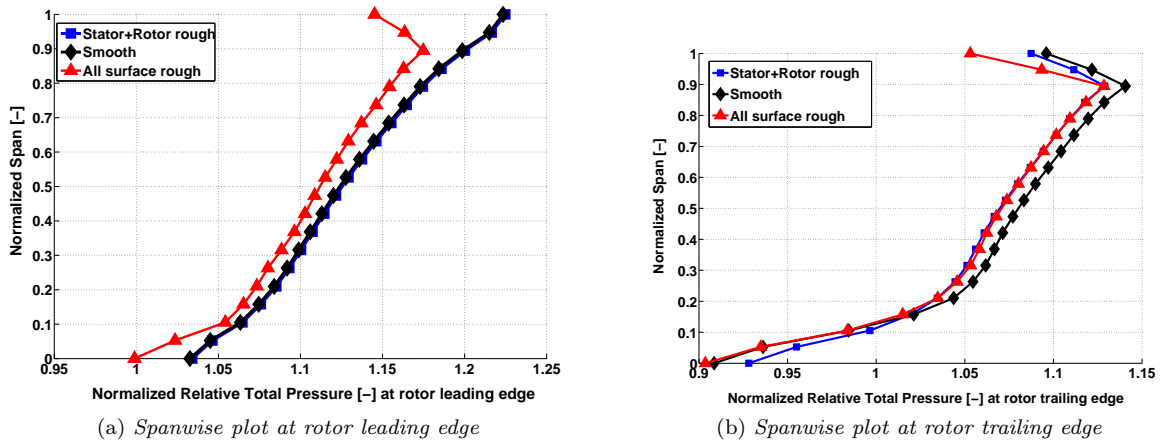


Figure 4.16: Spanwise plot for all cases for rotor blade

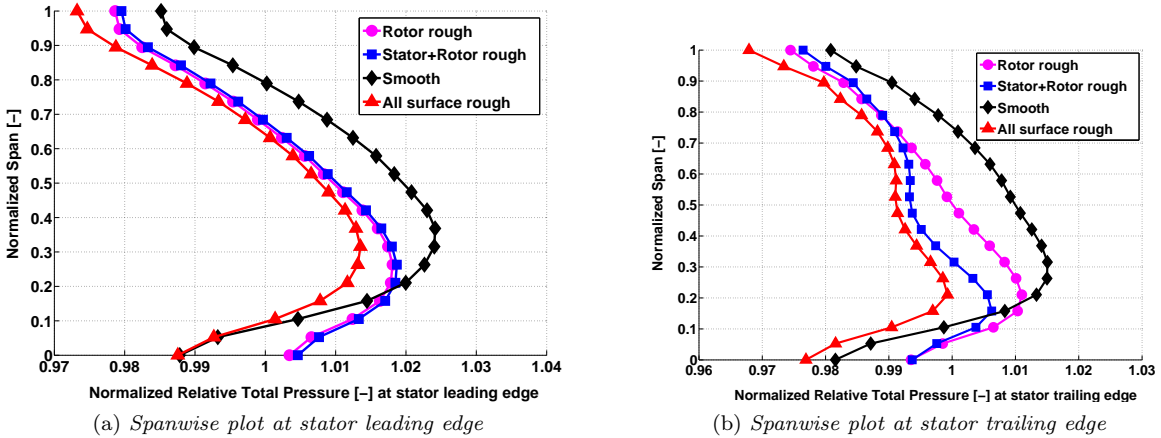


Figure 4.17: Spanwise plot for all cases for stator blade

The blade to blade section contour plot of the Mach number for the mid span section is shown in fig. 4.18a to fig.4.18c and for the near hub section in the fig.4.19a to 4.19c respectively. The plots 4.18b -4.18c shows the increase in wake near the trailing edge of the stator for the rough case compared to the smooth case through the mid-span sections. The decrease in separation near the hub region of the rotor blade suction side with roughness can be seen in 4.19b & 4.19c through the variations in the gradient. But the separation is then increased with the introduction of surface roughness on the hub and shroud as seen in fig 4.18c.

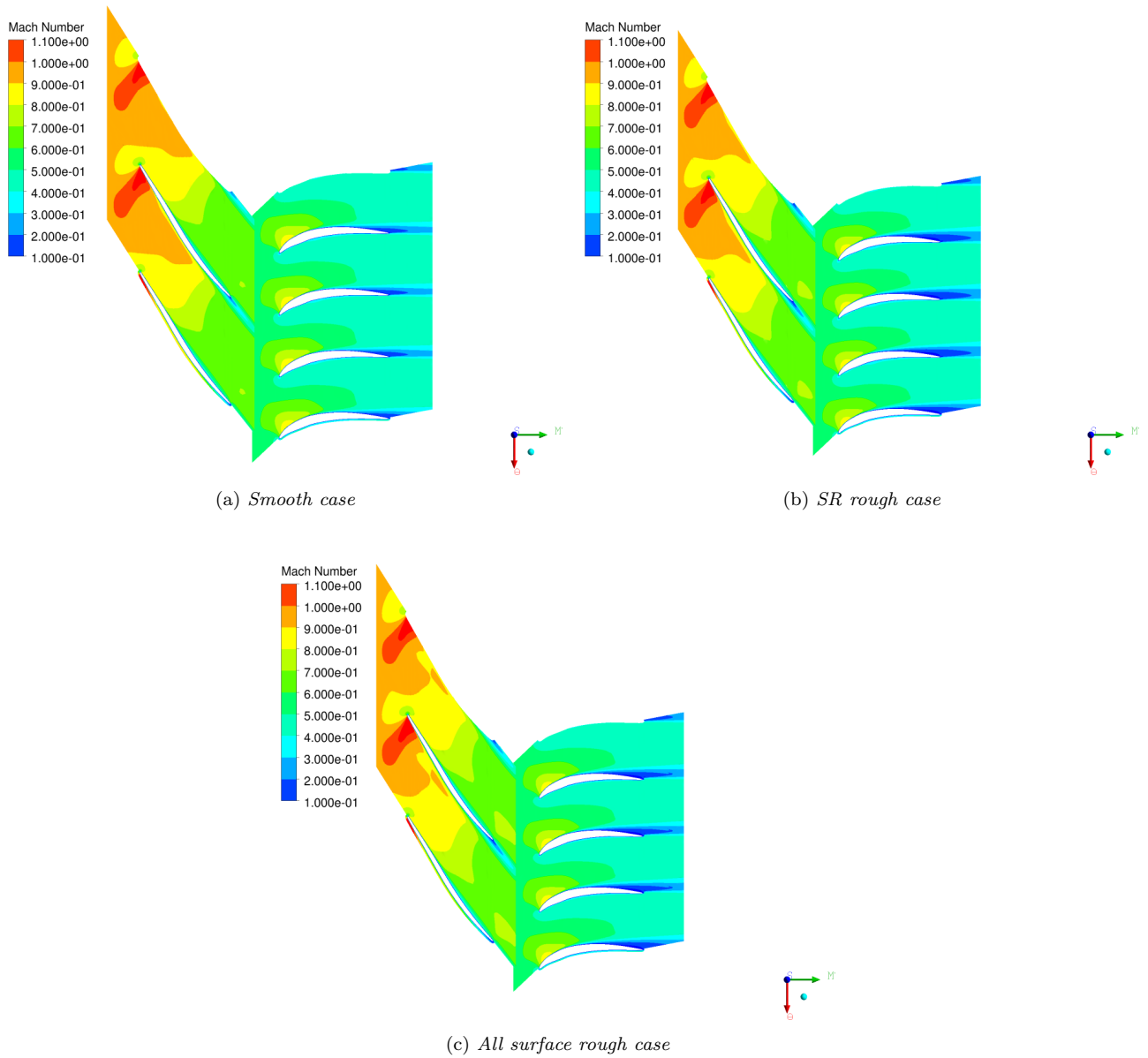


Figure 4.18: Mach number contours at the Mid Section (MS) of the span

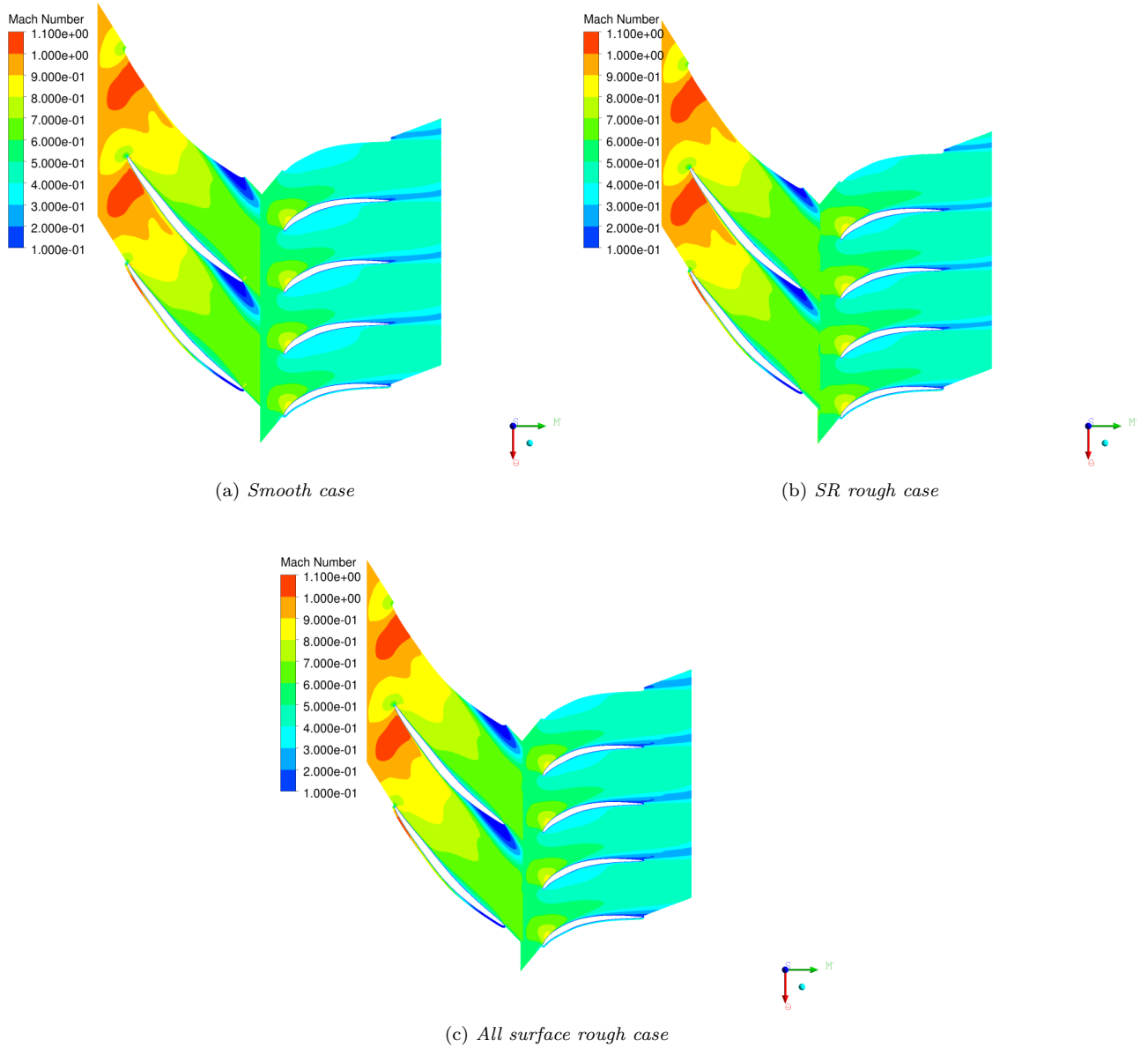


Figure 4.19: Mach number contours at the Near Hub(NH) section of the span

4.4 Transition influence on the Stage performance

The effect of transition on the transonic compressor stage performance was investigated by enabling the transition modeling in ANSYS CFX. The transition settings were the same as described in 2D Transition simulations. The mesh used for the transition simulations is a Low Reynolds grid. The figure 4.20 shows the compressor map comparing the steady state simulations for the transonic compressor stage with and without transition. The transition simulations were done for smooth case and rough case where the rough case is done for maximum roughness size $25\mu\text{m}$ on both rotor and stator blades. The influence of transition was less on the performance of the stage with and without surface roughness. The inclusion of transition along with turbulence modeling have very less effect on the performance of the compressor stage.

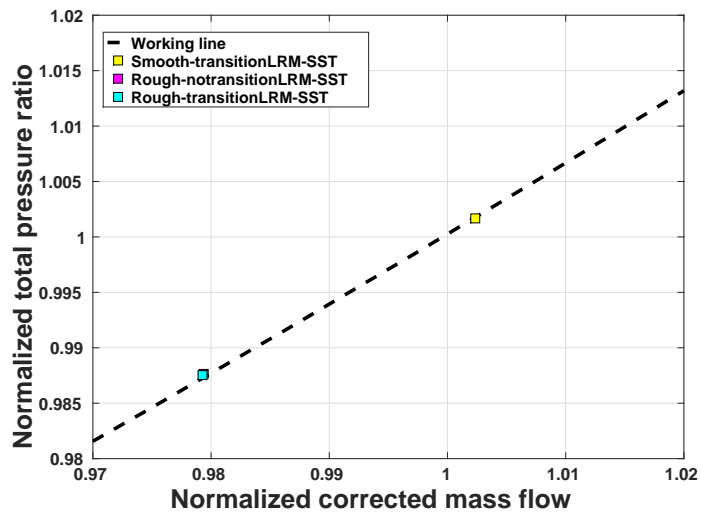


Figure 4.20: Compressor map from the transition simulations

Chapter 5

Conclusion

5.1 Summary and Conclusion

The performance deterioration in a transonic compressor stage due to surface roughness was investigated through CFD simulations. A 2D analysis was done to evaluate the existing surface models in ANSYS CFX and ANSYS Fluent. Results for a NACA 0012 airfoil was compared with the experimental data from a NACA report[14]. The lift and drag coefficients C_l and C_d were evaluated with and without surface roughness. The change in drag coefficient from the ANSYS CFX and ANSYS FLUENT results were compared to the experimental data from which it was inferred that ANSYS CFX values followed the same trend as the experimental data. Further simulations for a transonic compressor stage were carried out in ANSYS CFX for different sand grain roughness sizes ranging from $1\mu\text{m}$ to $25\mu\text{m}$ compared to the smooth case. The effect of surface roughness was more pronounced for the polytropic efficiency compared to other performance parameters which were total pressure ratio and corrected mass flow. About 2.6 % loss in polytropic efficiency was resulted for maximum surface roughness size of $25\mu\text{m}$. The results from the stage performance evaluation showed a decrease in all performance parameters with the inclusion of surface roughness on the blades.

The flow field over the stage domain was analysed by surface streamlines and contour plots. The analysis showed a reduction in decline of relative total pressure near the rotor hub region and thicker wake near the stator mid span region due to roughness. An increase in wake was found near the mid span region of rotor and stator suction side. The pressure side of the blades were less affected due to the roughness on the surfaces. The radial distribution of the relative total pressure showed the decrease in separation near the rotor hub region with the influence of roughness. The transition, both with and without surface roughness was found to have a negligible effect on the stage performance.

5.2 Future work

Future work will include integration of the surface roughness model into an optimization framework of compressor blades. The findings from the analysis of the stage compressor needs to be validated with experimental data. Furthermore, the transient simulations could be performed to investigate the transient effects of the surface roughness on the performance of the compressor stage. Influence of surface roughness with boundary layer transition needs to be further studied more deeply. Analysis of surface roughness on the local regions such as leading edge of the blades can be done. The effect of Reynolds number and free stream turbulence level on the surface roughness would give some insights into the off-design conditions which involves low-Re modelling and on-design conditions. The effect of tip clearance along with surface roughness will provide more information about the end wall boundary layers.

References

- [1] S. Peng and P. Eliasson, “Some remarks on cfd drag prediction of an aircraft model”, *New Trends in Fluid Mechanics Research*, Springer, 2009, pp. 214–217.
- [2] D. C. Eleni, T. I. Athanasios, and M. P. Dionissios, Evaluation of the turbulence models for the simulation of the flow over a national advisory committee for aeronautics (naca) 0012 airfoil, *Journal of Mechanical Engineering Research* vol. 4, no. 3 2012, 100–111, 2012.
- [3] E. Castiñeira-Martínez, I. Solís-Gallego, J. González, J. F. Oro, K. A. Díaz, and S. Velarde-Suárez, Application of computational fluid dynamics models to aerodynamic design and optimization of wind turbine airfoils,
- [4] J. Denton, Lessons from rotor 37, *Journal of Thermal Science* vol. 6, no. 1 1997, 1–13, 1997.
- [5] L. Ellbrant, *Multi-objective CFD-based Design Method for Axial Compressors*. 2014.
- [6] K. Bammert and G. Woelk, The influence of the blading surface roughness on the aerodynamic behavior and characteristic of an axial compressor, *Journal of Engineering for Gas Turbines and Power* vol. 102, no. 2 1980, 283–287, 1980.
- [7] T. Adams, C. Grant, and H. Watson, A simple algorithm to relate measured surface roughness to equivalent sand-grain roughness, *Journal ISSN* vol. 2929 2012, 2724, 2012.
- [8] L. Ellbrant, *DERIVATION OF THE WORKING LINE FOR A COMPRESSOR WITH AN EXIT THROTTLE*. 2014.
- [9] S. C. Back, J. H. Sohn, and S. J. Song, Impact of surface roughness on compressor cascade performance, *Journal of Fluids Engineering* vol. 132, no. 6 2010, 064502, 2010.
- [10] S. C. Back, G. V. Hobson, S. J. Song, and K. T. Millsaps, Effects of reynolds number and surface roughness magnitude and location on compressor cascade performance, *Journal of Turbomachinery* vol. 134, no. 5 2012, 051013, 2012.
- [11] K. L. Suder, R. V. Chima, A. J. Strazisar, and W. B. Roberts, The effect of adding roughness and thickness to a transonic axial compressor rotor, *Journal of turbomachinery* vol. 117, no. 4 1995, 491–505, 1995.
- [12] S. A. Gbadebo, T. P. Hynes, and N. A. Cumpsty, “Influence of surface roughness on three-dimensional separation in axial compressors”, *ASME Turbo Expo 2004: Power for Land, Sea, and Air*, American Society of Mechanical Engineers, 2004, pp. 471–481.
- [13] W. Elrod, P. King, and E. Poniowski, “Effects of surface roughness, freestream turbulence, and incidence angle on the performance of a 2-d compressor cascade”, *ASME, International Gas Turbine and Aeroengine Congress and Exposition, 35 th, Brussels, Belgium*, 1990, p. 1990.
- [14] R. W. Hooker, *The aerodynamic characteristics of airfoils as affected by surface roughness*. National Advisory Committee for Aeronautics, 1933.
- [15] K. Bammert and H. Sandstede, “Influences of manufacturing tolerances and surface roughness of blades on the performance of turbines”, *American Society of Mechanical Engineers, Gas Turbine Conference and Products Show, Houston, Tex*, 1975, p. 1975.
- [16] S. Chen, S. Sun, H. Xu, L. Zhang, S. Wang, and T. Zhang, “Influence of local surface roughness of rotor blade on performance of an axial compressor stage”, *ASME Turbo Expo 2013: Turbine Technical Conference and Exposition*, American Society of Mechanical Engineers, 2013, V06AT35A015–V06AT35A015.
- [17] R. Leipold, M. Boese, and L. Fottner, The influence of technical surface roughness caused by precision forging on the flow around a highly loaded compressor cascade, *ASME J. Turbomach* vol. 122, no. 3 2000, 416–425, 2000.
- [18] E. Syverud and L. E. Bakken, “The impact of surface roughness on axial compressor performance deterioration”, *ASME Turbo Expo 2006: Power for Land, Sea, and Air*, American Society of Mechanical Engineers, 2006, pp. 491–501.
- [19] S.-H. Kang, Y.-S. Kang, and K.-H. Han, “Numerical study on blade roughness effect on the performance of turbomachines”, *Proceedings International Gas Turbine Congress, Tokyo, Japan*, 2003, pp. 2–7.
- [20] A. Schaffler, Experimental and analytical investigation of the effects of reynolds number and blade surface roughness on multistage axial flow compressors, *Journal of Engineering for Gas Turbines and Power* vol. 102, no. 1 1980, 5–12, 1980.

- [21] J. H. Im, J. H. Shin, G. V. Hobson, S. J. Song, and K. T. Millsaps, "Effect of leading edge roughness and reynolds number on compressor profile loss", *ASME Turbo Expo 2013: Turbine Technical Conference and Exposition*, American Society of Mechanical Engineers, 2013, V06AT35A034–V06AT35A034.
- [22] J. Denton, Lessons from rotor 37, *Journal of Thermal Science* vol. **6**, no. 1 1997, 1–13, 1997.
- [23] T. Bai, J. Liu, W. Zhang, and Z. Zou, Effect of surface roughness on the aerodynamic performance of turbine blade cascade, *Propulsion and Power Research* vol. **3**, no. 2 2014, 82–89, 2014.
- [24] J. D. Denton, "Some limitations of turbomachinery cfd", *ASME Turbo Expo 2010: Power for Land, Sea, and Air*, American Society of Mechanical Engineers, 2010, pp. 735–745.
- [25] C. B. Meher-Homji, M. Chaker, and H. Motiwalla, "Gas turbine performance deterioration", *Proceedings of the 30th Turbomachinery Symposium*, 2001, pp. 17–20.
- [26] H. Yang and H. Xu, The effect of blade profile parameter on thermodynamic performance parameter of axial flow compressor, *International Journal of Computer Applications in Technology* vol. **50**, no. 3-4 2014, 247–252, 2014.
- [27] N. A. Cumpsty, *Compressor aerodynamics*. Longman Scientific & Technical, 1989.
- [28] J. D. Anderson, *COMPUTATIONAL FLUID DYNAMICS: The Basics with Applications*. McGraw-Hill, 1995.
- [29] S. L. Dixon and C. Hall, *Fluid mechanics and thermodynamics of turbomachinery*. Butterworth-Heinemann, 2013.
- [30] H. Schlichting, K. Gersten, and K. Gersten, *Boundary-layer theory*. Springer Science & Business Media, 2000.
- [31] L. Davidson *et al.*, *An introduction to turbulence models*. Department of Thermo and Fluid Dynamics, Chalmers University of Technology, Gothenburg, Sweden, 2003.
- [32] C. Koch and L. Smith, Loss sources and magnitudes in axial-flow compressors, *Journal of Engineering for Gas Turbines and Power* vol. **98**, no. 3 1976, 411–424, 1976.
- [33] *Cfx and fluent manual, Wall roughness modelling*, ANSYS, 2013. [Online]. Available: <http://148.204.81.206/Ansys/readme.html>.
- [34] *Cfx anf fluent forums, Wall roughness modelling*, cfd-online. [Online]. Available: <http://www.cfd-online.com/Forums/>.
- [35] *Gas turbine compressor blade fouling mechanisms*, Pipeline and GasJournal, 2011. [Online]. Available: <http://www.pipelineandgasjournal.com/gas-turbine-compressor-blade-fouling-mechanisms?page=show>.